

Identifying a Training-Set Attack’s Target Using Renormalized Influence Estimation

Zayd Hammoudeh

Daniel Lowd

University of Oregon

ABSTRACT

Targeted training-set attacks inject malicious instances into the training set to cause a trained model to mislabel one or more specific test instances. This work proposes the task of *target identification*, which determines whether a specific test instance is the target of a training-set attack. This can then be combined with *adversarial-instance identification* to find (and remove) the attack instances, mitigating the attack with minimal impact on other predictions. Rather than focusing on a single attack method or data modality, we build on influence estimation, which quantifies each training instance’s contribution to a model’s prediction. We show that existing influence estimators’ poor practical performance often derives from their over-reliance on instances and iterations with large losses. Our *renormalized* influence estimators fix this weakness; they far outperform the original ones at identifying influential groups of training examples in both adversarial and non-adversarial settings, even finding up to 100% of adversarial training instances with no clean-data false positives. Target identification then simplifies to detecting test instances with anomalous influence values. We demonstrate our method’s generality on backdoor and poisoning attacks across various data domains including text, vision, and speech. Our source code is available at https://github.com/ZaydH/target_identification.

1 INTRODUCTION

Targeted training-set attacks manipulate an ML system’s prediction on one or more *target* test instances by maliciously modifying the training data [2, 20, 27, 45, 59, 60, 68]. For example, a retailer may attempt to trick a spam filter into mislabeling all of a competitor’s emails as spam [60]. Targeted attacks require very few corrupted instances [68], and their effect on the test error is quite small, making them harder to detect [10] than *availability training-set attacks* [10], which seek to degrade an ML system’s overall performance [7, 18, 72].

Kumar et al. [35] survey business and governmental organizations and find that training-set attacks were the top ML security concern, due to previous successful attacks [36]. Kumar et al. specifically identify defenses against such attacks as a significant, practical gap. Existing training-set defenses [19, 50, 73] change the training procedure to mitigate the impact of an attack but provide little information about the attacker’s goals, methods, or identity. Learning more about the attacker is essential for anticipating their attacks [51], designing targeted defenses [1], and even building defenses outside the ML system, such as stopping spammers through their payment processors [37].

This paper’s defense against training-set attacks focuses on the related goals of learning more about an attacker and stopping their attacks. We achieve this through a pair of related tasks:

- (1) *target identification*: identifying the target of a training-set attack, which may provide insight into the attacker’s goals and how to defend against them; and
- (2) *adversarial-instance identification*: identifying the malicious instances that constitute the training-set attack.

We are not aware of any work that studies training-set attack target identification beyond very simple attacks.

Our *key insight* is the synergistic interplay between the two tasks above. If attackers can add only a limited number of training instances (as is often the case) [10, 60, 68], then these malicious instances must be highly influential to change target predictions. Thus, targets are those test instances with an unusual number of highly influential training examples. In contrast, non-targets tend to have many weak influences and few very strong ones. Thus, if we can (1) determine which instances influence which predictions and (2) detect outliers in this distribution, then we can jointly solve both tasks.

Unfortunately, determining which training instances are responsible for which model behaviors remains a challenge, especially for complex, black-box models such as neural networks. *Influence estimation* methods [11, 16, 31, 52, 74] attempt to quantify how much each training example contributes to a particular prediction, but current methods are brittle and often perform poorly [4, 5, 76].

This paper identifies a weakness common to many influence estimators [11, 31, 52, 74]: they induce a *low-loss penalty* that implicitly ranks confidently-predicted training instances as uninfluential. As a result, these methods systematically overlook (groups of) highly influential, low-loss instances. We remedy this via a simple *renormalization* that removes the low-loss penalty. Our new *renormalized influence estimators* consistently outperform the originals in both adversarial and non-adversarial settings. The most effective of these, *gradient aggregated similarity* (GAS), can often detect 100% of malicious training instances with no clean-data false positives.

Our *framework* for identifying targets of training-set attacks, FIT, compares the distribution of influence values across test instances checking for outliers. More concretely, FIT marks as potential targets those test instances with an unusual number of highly influential instances as explained above. Next, FIT mitigates the attack’s effect by removing exceptionally influential training instances associated with the target(s). Since mitigation considers only targets, training instance outliers that are “helpful” to non-targets are unaffected. This *target-driven mitigation* has a positive or neutral effect on clean data yet is highly effective on adversarial data where finding even a single target suffices to disable the attack on almost all other targets.

Correspondence to: zayd@cs.uoregon.edu. This is an extended and extensively revised version of a paper presented at the ICML 2021 Workshop on Uncertainty and Robustness in Deep Learning (UDL) [24].

By relying on the concepts of influence estimation and not the properties of a particular attack or domain, GAS and FIT are *attack agnostic* [58]. They can apply equally well to different attack types, including *data poisoning* attacks, which target unperturbed test data, and *backdoor* attacks on test instances activating a specific trigger. Our approach works across data domains from CNN image classifiers to speech recognition to even text models based on transformers. Such agnosticism is both more challenging and more useful in practice since it is not readily bypassable.

In addition to learning more about the attack and attacker, *target identification enables targeted mitigation*. Certified training-set defenses [29, 38, 63, 70] (which do not identify targets) implement countermeasures (e.g., smoothing) that affect predictions on *all* instances – not just the very few targets. These methods can substantially degrade performance, in some cases causing up to 10× more errors on clean data [18]. A strength of deep neural networks is that they can “memorize” instances to learn rare cases from one or two examples [16]; certified training prevents this by limiting any single training instance’s influence.

Our work’s contributions are enumerated below. Note that additional experiments and the proof are in the supplemental materials.

- (1) We identify a weakness common to all loss-based influence estimators and provide a simple renormalization correction that addresses this weakness.
- (2) Inspired by influence estimation, we propose GAS – a renormalized influence estimator that is highly adept at identifying influential groups of training instances.
- (3) Leveraging techniques from anomaly detection and *robust statistics*, we extend GAS into a general framework for identifying targets of training-set attacks, FIT.
- (4) We use GAS in a target-driven data sanitizer that mitigates attacks while removing very few clean instances.
- (5) We demonstrate the effectiveness and attack agnosticism of GAS and FIT on a diverse set of attacks and data modalities, including speech recognition, vision, and text.

In the remainder of the paper, we begin by establishing notation and reviewing prior work (Sections 2 and 3). Then in Section 4, we show how existing influence estimators are inadequate for identifying (groups of) highly influential training instances. We also introduce our renormalization fix for influence estimation and describe our renormalized influence estimators. Section 5 builds on these improved influence estimates to define a framework for identifying the targets of an attack and mitigating the effect of the attack. We demonstrate the effectiveness of these methods in Section 6.

2 PROBLEM FORMULATION

Notation $x \in \mathcal{X}$ denotes a *feature vector* and $y \in \mathcal{Y}$ a *label*. *Training set*, $\mathcal{D}_{\text{tr}} = \{z_i\}_{i=1}^n$, consists of n training example tuples $z_i := (x_i, y_i)$. Consider *model* $f : \mathcal{X} \rightarrow \mathcal{A}$ parameterized by θ , where $a := f(x; \theta)$ denotes the model’s output (pre-softmax) *activations*. θ_0 denotes f ’s initial parameters, which may be randomly set and/or pre-trained.

For *loss function* $\ell : \mathcal{A} \times \mathcal{Y} \rightarrow \mathbb{R}_{\geq 0}$, denote z ’s empirical risk given θ as $\mathcal{L}(z; \theta) := \ell(f(x; \theta), y)$.¹ Consider any iterative, first-order optimization algorithm (e.g., gradient descent, Adam [30]). At each iteration $t \in \{1, \dots, T\}$, the optimizer updates parameters θ_t

¹Model f ’s output activation (e.g., softmax) is considered part of loss function ℓ .

from loss ℓ , previous parameters θ_{t-1} , and batch $\mathcal{B}_t \subseteq \mathcal{D}_{\text{tr}}$ of size b . Gradients are denoted $g_i^{(t)} := \nabla_{\theta} \mathcal{L}(z_i; \theta_t)$; superscript “(t)” is dropped when the iteration is clear from context.

Let $\tilde{z}_{\text{te}} := (x_{\text{te}}, \hat{y}_{\text{te}})$ be any *a priori* unknown test instance, where \hat{y}_{te} is the final model’s predicted label for x_{te} . Observe that \hat{y}_{te} may not be x_{te} ’s *true label*. Notation $\hat{\cdot}$ (e.g., \hat{z}, \hat{y}) denotes that the final predicted label $\hat{y} = f(x; \theta_T)$ is used in place of x ’s true label y .

Threat Model

The attacker crafts an *adversarial set* of perturbed instances, $\mathcal{D}_{\text{adv}} \subset \mathcal{D}_{\text{tr}}$. Denote the *clean training set* $\mathcal{D}_{\text{cl}} := \mathcal{D}_{\text{tr}} \setminus \mathcal{D}_{\text{adv}}$. We only consider successful attacks, as defined below.

Attacker Objective & Knowledge Let $\mathcal{X}_{\text{targ}} := \{x_j\}_{j=1}^m$ be a set of target feature vectors with shared true label $y_{\text{targ}} \in \mathcal{Y}$. The attacker crafts \mathcal{D}_{adv} to induce the model to mislabel all of $\mathcal{X}_{\text{targ}}$ as *adversarial label* y_{adv} . $\tilde{\mathcal{Z}}_{\text{targ}} := \{(x_j, y_{\text{adv}}) : x_j \in \mathcal{X}_{\text{targ}}\}$ denotes the *target set* and $\tilde{z}_{\text{targ}} := (x_{\text{targ}}, y_{\text{adv}})$ an arbitrary target instance. To avoid detection, the attacked model’s clean-data performance should be (essentially) unchanged. *Data poisoning* attacks only perturb adversarial set \mathcal{D}_{adv} . Target feature vectors are unperturbed/benign [7, 28, 45, 68]. *Clean-label poisoning* leaves labels unchanged when crafting \mathcal{D}_{adv} from seed instances [77]. *Backdoor* attacks perturb the features of both \mathcal{D}_{adv} and $\mathcal{X}_{\text{targ}}$ – often with the same *adversarial trigger* (e.g., change a specific pixel to maximum value). Generally, these triggers can be inserted into any test example targeted by the adversary, making most backdoor attacks *multi-target* ($|\tilde{\mathcal{Z}}_{\text{targ}}| > 1$) [22, 41, 65, 70]. \mathcal{D}_{adv} ’s labels may also be changed.

To ensure the strongest adversary, the attacker knows any pre-trained initial parameters. Where applicable, the attacker also knows the training hyperparameters and clean dataset \mathcal{D}_{cl} . Moreover, the attacker’s computational resources are not constrained when crafting \mathcal{D}_{adv} . The attacker never knows the batch sequence nor any randomly-set initial parameters (e.g., the classification layer).

Defender Objective & Knowledge Let $\tilde{\mathcal{Z}}_{\text{te}}$ denote a set of *a priori* unknown test examples. These are the instances the defender is concerned about enough to analyze as potential targets.² Our goals are to (1) *identify* any attack targets in $\tilde{\mathcal{Z}}_{\text{te}}$, and (2) *mitigate* the attack by removing the adversarial instances \mathcal{D}_{adv} associated with those target(s). No assumptions are made about the modality/domain (e.g., text, vision) or adversarial perturbation (e.g., whether an attack is backdoor or data poisoning). We do not assume access to clean validation data.

3 RELATED WORK

We mitigate training-set attacks by building upon influence estimation to identify the target(s) and adversarial set. This section first reviews existing defenses against training-set attacks and then formalizes training-set influence as defined in previous work.

3.1 Defenses Against Training-Set Attacks

Certifiably-robust defenses [29, 63, 70] provide (limited) theoretically-guaranteed protection against specific training-set attacks under specific assumptions. *Empirical defenses* [15, 19, 50, 66, 78, 79] derive from understandings and observations about the underlying

²Generally, there are far fewer potential targets ($\tilde{\mathcal{Z}}_{\text{te}}$) than possible test examples.

mechanisms training-set attacks exploit to change a network’s predictions. In practice, empirical defenses generally significantly outperform certified approaches with fewer harmful side effects – albeit without a guarantee [40]. These two defense categories are complementary and can be deployed together for better performance. Since our defense is largely empirical, we focus on that defense category below.

We are not aware of any existing defense – certified or empirical – that provides target identification. The most closely related task is determining whether a model is infected with a backdoor, which ignores poisoning and other training-set attacks [62, 73]. Such methods make different assumptions than this work. For instance, they assume access to a known-clean validation set but not to the full training set \mathcal{D}_{tr} . Many also make additional assumptions about the type of attack or the training methodology [62].

Another task similar to target identification is *adversarial trigger synthesis*, which attempts to reconstruct any backdoor attack pattern(s) a model learned [19, 66, 67, 79]. These methods mitigate attacks by adding any identified pattern(s) to known-clean data expecting that retraining will cause catastrophic forgetting of the trigger(s). We are not aware of any work examining the use of (non-trivial) reconstructed triggers to detect backdoored test instances. In practice, the synthesized triggers only approximately align with the actual adversarial triggers and are often just universal triggers [53]. Therefore, whether these methods could act as reliable backdoor target identifiers is an open question. Trigger synthesis does not apply to poisoning attacks.

In contrast to trigger synthesis methods which stop attacks by creating new training instances, *data-sanitization* defenses mitigate attacks by removing adversarial set \mathcal{D}_{adv} from \mathcal{D}_{tr} . Existing data-sanitization defenses have shown promise [9, 50, 65], but they all share a common pitfall concerning setting the data-removal threshold [32, 40]. If this threshold is set too low, significant clean-data removal degrades overall clean-data performance. A threshold set too high results in insufficient adversarial training data removal and the attack remaining successful. Additional information (e.g., target identification) enables targeted tuning of this removal threshold.

Most existing certified and empirical defenses are not attack agnostic and assume specific data modalities (e.g., only vision [19, 66, 67, 79]), model architectures (e.g. CNNs [33]), optimizers [25], or training paradigms [62]. Attack agnosticism is more challenging and more practically useful. We achieve agnosticism by building upon existing methods that are general – specifically influence estimation, which is formalized next.

3.2 Training-Set Influence Estimation

In every successful attack, the added training instances change the model’s prediction for a particular input. If the attacker can only add a limited number of instances (e.g., 1% of \mathcal{D}_{tr}), these instances must be highly influential to accomplish the attacker’s goal.

Influence estimation’s goal is to determine which training instances are most responsible for a learned model’s parameters, performance on test data, or prediction for a particular input. This is often viewed as a counterfactual: which instance (or group of instances) induces the biggest change when removed from the training data? While there are multiple definitions of influence,

as detailed below, influence estimation methods can be broadly viewed as quantifying the relative responsibility of each training instance $z_i \in \mathcal{D}_{\text{tr}}$ on some test prediction $f(\widehat{z}_{\text{te}}; \theta_T)$.

Static influence estimators consider only (a subset of) the final model parameters θ_T . For example, Koh and Liang’s [31] seminal work defines influence, $I_{\text{IF}}(z_i, \widehat{z}_{\text{te}})$, as the change in risk $\mathcal{L}(\widehat{z}_{\text{te}}; \theta_T)$ if $z_i \notin \mathcal{D}_{\text{tr}}$, i.e., the leave-one-out (LOO) change in test loss. By assuming model strict convexity and stationarity, Koh and Liang’s *influence functions* estimator approximates this LOO influence as

$$I_{\text{IF}}(z_i, \widehat{z}_{\text{te}}) \approx \frac{1}{n} \nabla_{\theta} \mathcal{L}(\widehat{z}_{\text{te}}; \theta_T)^{\top} H_{\theta}^{-1} \nabla_{\theta} \mathcal{L}(z_i; \theta_T), \quad (1)$$

with H_{θ}^{-1} the inverse of risk Hessian $H_{\theta} := \frac{1}{n} \sum_{z_i \in \mathcal{D}_{\text{tr}}} \nabla_{\theta}^2 \mathcal{L}(z_i; \theta_T)$.

Yeh et al. [74]’s *representer point* static estimator exclusively considers the model’s final, linear classification layer. All preceding layers are treated as a fixed feature-extractor. Let \mathbf{f}_i denote x_i ’s penultimate feature representation w.r.t. final parameters θ_T . Then the representer point influence of $z_i \in \mathcal{D}_{\text{tr}}$ on \widehat{z}_{te} is

$$I_{\text{RP}}(z_i, \widehat{z}_{\text{te}}) := -\frac{1}{2\lambda n} \left(\frac{\partial \mathcal{L}(z_i; \theta_T)}{\partial a_{y_i}} \right) \langle \mathbf{f}_i, \mathbf{f}_{\text{te}} \rangle, \quad (2)$$

where $\lambda > 0$ is the weight decay (L_2) regularizer and $\langle \cdot, \cdot \rangle$ denotes vector dot product. Scalar $\frac{\partial \mathcal{L}(z_i; \theta_T)}{\partial a_{y_i}}$ is the partial derivative of risk \mathcal{L} w.r.t. activation a ’s y_i -th dimension at a .

Dynamic influence estimators measure influence based on how losses change during training. More formally, influence is quantified according to how batches $\mathcal{B}_1, \dots, \mathcal{B}_T$ affect model parameters $\theta_0, \dots, \theta_T$ and by consequence risks $\mathcal{L}(\cdot; \theta_0), \dots, \mathcal{L}(\cdot; \theta_T)$. For example, Pruthi et al.’s [52] *TracIn* estimates influence by “tracing” training – aggregating changes in \widehat{z}_{te} ’s test loss each time training example z_i ’s gradient updates parameters θ_t . For stochastic gradient descent (batch size $b = 1$), z_i ’s TracIn influence on \widehat{z}_{te} is

$$I_{\text{TracIn}}(z_i, \widehat{z}_{\text{te}}) := \sum_{t=1}^T \mathbb{1}_{z_i \in \mathcal{B}_t} \left(\mathcal{L}(\widehat{z}_{\text{te}}; \theta_{t-1}) - \mathcal{L}(\widehat{z}_{\text{te}}; \theta_t) \right), \quad (3)$$

where $\mathbb{1}_u$ is the indicator function s.t. $\mathbb{1}_u = 1$ if predicate u is true and 0 otherwise. Pruthi et al. approximate Eq. (3) as,

$$I_{\text{TracIn}}(z_i, \widehat{z}_{\text{te}}) \approx \sum_{z_i \in \mathcal{B}_t} \frac{\eta_t}{b} \left\langle \nabla_{\theta} \mathcal{L}(z_i; \theta_{t-1}), \nabla_{\theta} \mathcal{L}(\widehat{z}_{\text{te}}; \theta_{t-1}) \right\rangle, \quad (4)$$

where η_t is iteration t ’s learning rate.

Suppl. Algorithm 4³ details the minimal changes made to model training to support TracIn where $\mathcal{T} \subset \{1, \dots, T\}$ is a preselected *subset of training iterations* and $\mathcal{P} := \{(\eta_t, \theta_{t-1}) : t \in \mathcal{T}\}$ is the *serialized training parameters*. Algorithm 5 outlines TracIn’s influence estimation procedure for *a priori* unknown test instance \widehat{z}_{te} . Influence vector \mathbf{v} ($|\mathbf{v}| = n$) contains the TracIn influence estimates for each $z_i \in \mathcal{D}_{\text{tr}}$. Generally, $|\mathcal{T}| \ll T$, and \mathcal{T} is evenly-spaced in $\{1, \dots, T\}$, meaning in practice, TracIn effectively treats multiple batches like a single model update.

Pruthi et al. also propose *TracIn Checkpoint* (TracInCP) – a more heuristic version of TracIn that considers *all* training examples at each checkpoint in \mathcal{T} , not just those instances in the intervening batches, as shown in Algorithm 1.⁴ Formally,

$$I_{\text{TracInCP}}(z_i, \widehat{z}_{\text{te}}) := \sum_{t \in \mathcal{T}} \frac{\eta_t}{b} \left\langle \nabla_{\theta} \mathcal{L}(z_i; \theta_{t-1}), \nabla_{\theta} \mathcal{L}(\widehat{z}_{\text{te}}; \theta_{t-1}) \right\rangle. \quad (5)$$

³Due to space, Algorithms 4 and 5 appear in the supplementals.

⁴Algorithm 1 combines two different methods TracInCP and our renormalized version, GAS, detailed in Section 4.3.

TracInCP is more computationally expensive than TracIn – with the slowdown linear w.r.t. the number of checkpoints per epoch.

A major advantage of TracIn and TracInCP over other estimators (e.g., influence functions) is that their only hyperparameter is iteration set \mathcal{T} , which we tuned based only on compute availability.

Chen et al.’s [11] HyDRA is an additional dynamic influence estimator. However, HyDRA’s $O(n|\theta|)$ memory complexity makes it impractical. We focus on TracIn as its memory complexity is only $O(n)$. HyDRA and TracIn were published contemporaneously and share the same core idea. Influence renormalization – proposed in the next section – also applies to HyDRA.

4 WHY INFLUENCE ESTIMATION OFTEN FAILS AND HOW TO FIX IT

Before addressing the task of target identification, we first consider the related task of adversarial-instance identification. In the simplest case, if the attack target is known, then the malicious instances should be among the most influential instances for that target instance. In other words, *adversarial-instance identification reduces to influence estimation*. However, the influence estimators above share a common weakness that makes them poorly suited for this task. They all consistently rank confidently-predicted training instances as uninfluential. We illustrate this behavior below using a simple, intuitive experiment. We then explain this weakness’s cause and propose a simple fix that addresses it on adversarial and non-adversarial data, for all preceding estimators. This fix is needed to successfully identify adversarial set \mathcal{D}_{adv} and, as detailed in Sec. 5, attack targets.

4.1 A Simple Experiment

Consider binary classification where clean set \mathcal{D}_{cl} is all frog and airplane training images in CIFAR10 ($|\mathcal{D}_{\text{cl}}| = 10,000$). To simulate a naive backdoor attack, adversarial set \mathcal{D}_{adv} is 150 randomly selected MNIST 0 images labeled as airplane. When trained on \mathcal{D}_{cl} , a state-of-the-art ResNet9 network [47] labels MNIST 0s as frog and airplane with very nearly the same frequency. In contrast, when training using $\mathcal{D}_{\text{tr}} := \mathcal{D}_{\text{adv}} \sqcup \mathcal{D}_{\text{cl}}$, MNIST 0 test instances were always classified as airplane, meaning \mathcal{D}_{adv} is overwhelmingly influential on MNIST predictions. This is expected given the huge difference between the MNIST and CIFAR10 data distributions.

We used this simple setup to evaluate different influence estimation methods. We first trained 30 randomly-initialized networks using the above datasets and binary cross-entropy loss. We then performed influence estimation on each network for a randomly selected MNIST 0 test instance to determine how well each estimator identified adversarial set \mathcal{D}_{adv} .⁵ Given the large imbalance between the amount of clean and “adversarial” data, i.e., $|\mathcal{D}_{\text{adv}}| \ll |\mathcal{D}_{\text{cl}}|$, performance is measured using area under the precision-recall curve (AUPRC), which quantifies how well \mathcal{D}_{adv} ’s influence ranks relative to \mathcal{D}_{cl} . Precision-recall curves are preferred for highly-skewed classification tasks since they provide more insight into the false-positive rate [14].

The upper half of Figure 1 shows how well each influence estimator in Section 3.2 identifies \mathcal{D}_{adv} , both quantitatively and qualitatively. The dynamic estimators significantly outperformed their

static counterparts, with the more heuristic TracInCP as the overall top performer. However, no influence estimator consistently ranked MNIST training instances (i.e., \mathcal{D}_{adv}) in the top-5 most influential, with influence functions marking instances from the other class (frog) as most influential. Influence estimation’s poor performance here is particularly noteworthy as the task was designed to be unrealistically easy.

4.2 Why Influence Performs Poorly

Intra-training dynamics illuminate the root cause of influence estimation’s poor performance here. Figure 2 visualizes \mathcal{D}_{adv} ’s and \mathcal{D}_{cl} ’s training losses at each training checkpoint. It also plots the *gradient norm ratio* between the median adversarial and clean training instance gradient magnitude, which closely tracks the training sets’ loss values. Both during and at the end of training, \mathcal{D}_{adv} ’s median loss is significantly smaller than that of \mathcal{D}_{cl} – often by several orders of magnitude.

Low-Loss Penalty. Section 3.2’s influence estimators weight influence by $\frac{\partial \ell(a, y)}{\partial a}$ either directly (representer point (2)) or indirectly via the *chain rule* (influence functions (1) and TracIn (4) & (5)) as

$$\nabla_{\theta} \mathcal{L}(z; \theta) := \frac{\partial \ell(f(x), y)}{\partial x} = \frac{\partial \ell(a, y)}{\partial a} \cdot \frac{\partial a}{\partial x}. \quad (6)$$

Therefore, loss-based influence estimation *implicitly penalizes all training instances with low(er) training loss in the absolute (relative) sense*, e.g., \mathcal{D}_{adv} as shown in Figure 2.

Theorem 4.1 summarizes this relationship when there is a single output activation ($|a| = 1$), e.g., binary classification and univariate regression. In short, when Theorem 4.1’s conditions are met, loss induces a perfect ordering on the corresponding norm.

THEOREM 4.1. *Let loss function $\tilde{\ell} : \mathbb{R} \rightarrow \mathbb{R}_{\geq 0}$ be twice-differentiable and either even⁶ or monotonically increasing with $\forall_a \nabla_a^2 \tilde{\ell}(a) > 0$. Then, it holds that*

$$\tilde{\ell}(a) < \tilde{\ell}(a') \implies \|\nabla_a \tilde{\ell}(a)\|_2 < \|\nabla_a \tilde{\ell}(a')\|_2. \quad (7)$$

Loss functions satisfying Theorem 4.1’s conditions include binary cross-entropy (i.e., logistic) and quadratic losses. Theorem 4.1 generally applies to multiclass losses, but there are cases where the ordering is not perfect. Although Theorem 4.1 primarily relates to training instance gradients and losses, the theorem applies to test examples as well. Dynamic estimators apply a low-loss penalty to any *iteration* where test instance \hat{z}_{te} has low loss.

The preceding should not be interpreted to imply that large gradient magnitudes are unimportant. Quite the opposite, large gradients have large influences on the model. However, the approximations necessary to make influence estimation tractable go too far by often focusing almost exclusively on training loss – and by extension gradient magnitude – leading these estimators to systematically overlook training instances with smaller gradients.

Static vs. Dynamic Influence: In Figure 1, static estimators (representer point & influence functions) significantly underperformed dynamic estimators (TracIn & TracInCP) by up to an order of magnitude. Since static estimators only consider final model parameters θ_T , they only see the case where the loss penalty is high. In

⁵See supplemental Section C for the complete experimental setup details.

⁶“Even” denotes that the function satisfies $\forall_a \tilde{\ell}(a) = \tilde{\ell}(-a)$.



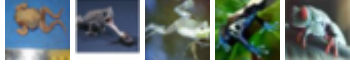






<div>Test Example</div> 	Method	AUPRC	Top-5 Highest Ranked
	Representer Point	0.030 ± 0.009	
	Influence Functions	0.029 ± 0.018	
	TracIn	0.140 ± 0.098	
	TracInCP	0.309 ± 0.260	
	Representer Point Renormalized (ours)	0.778 ± 0.144	
	Influence Functions Renormalized (ours)	0.215 ± 0.191	
	TracIn Renormalized (ours)	0.617 ± 0.115	
	GAS (ours) (TracInCP Renormalized)	0.977 ± 0.001	

Figure 1: Renormalized Influence: CIFAR10 & MNIST joint, binary classification for frog vs. airplane & MNIST 0 with $|\mathcal{D}_{cl}| = 10,000$ & $|\mathcal{D}_{adv}| = 150$. Influence estimators (upper half) consistently failed to rank \mathcal{D}_{adv} ’s MNIST training instances as highly influential on MNIST test instances. In contrast, all of our renormalized influence estimators (Section 4.3) outperformed their unnormalized version – with AUPRC improving up to 25 \times . Results averaged across 30 trials.

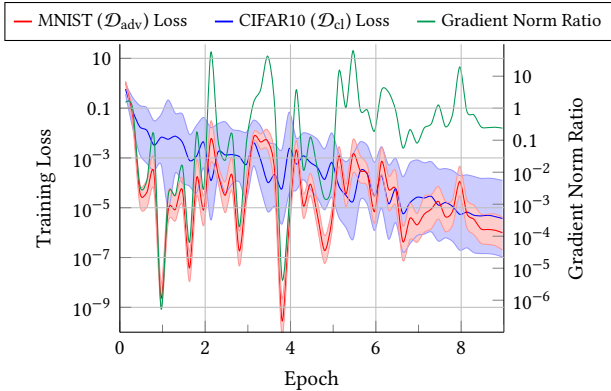


Figure 2: CIFAR10 & MNIST Intra-training Loss Tracking: \mathcal{D}_{adv} ’s (—) and \mathcal{D}_{cl} ’s (—) median cross-entropy losses (ℓ) at each training checkpoint for binary classification – frog vs. airplane & MNIST 0 – on ResNet9. The shaded regions correspond to each training set loss’s interquartile range. MNIST’s training losses are generally several orders of magnitude smaller than CIFAR10’s losses. Gradient norm ratio (—) demonstrates the tight coupling, throughout training, of loss and training gradient magnitude.

contrast, dynamic estimators consider all of training, including iterations where \mathcal{D}_{adv} ’s loss exceeds that of \mathcal{D}_{cl} . By (partially) avoiding this penalty, dynamic estimators perform better, albeit still poorly.

Derandomizing Dynamic Estimators: Among dynamic estimators, TracInCP significantly outperformed TracIn despite the latter being more theoretically sound. To understand why, imagine the training set contains two identical copies of some instance. In expectation, duplicates have equivalent influence on any test instance. However, TracIn assigns identical training examples different influence estimates based on their batch assignments with the difference potentially large depending on training dynamics. Figure 2 exhibits this principle where training loss fluctuates considerably intra-epoch. For example, \mathcal{D}_{adv} ’s median loss varies by more than seven orders of magnitude across the third epoch. TracIn’s low-loss penalty assigns significantly more influence to \mathcal{D}_{adv} instances early in that epoch compared to those later even though all MNIST instances should have relatively similar influence. By considering all examples at each checkpoint, TracInCP removes batch randomization’s direct effect on influence.⁷ Functionally, TracInCP simulates *influence expectation* without the need to train multiple models.

4.3 Renormalizing Influence Estimation

The CIFAR10 & MNIST joint classification experiment above demonstrates that a training example having low loss does *not* imply that it and related instances are uninfluential. Most importantly in the context of adversarial attacks, highly-related groups of (adversarial) instances may collectively cause those group members’ training

⁷Batch randomization still indirectly affects TracInCP and GAS (Sec. 4.3) through the model parameters. This effect could be mitigated by training multiple models and averaging (renormalized) influence, which is beyond the scope of this work.

Algorithm 1 GAS vs. TracInCP

Input: Training parameters \mathcal{P} , training set \mathcal{D}_{tr} , batch size b , and test example \widehat{z}_{te}

Output: (Renormalized) influence vector \mathbf{v}

```

1:  $\mathbf{v} \leftarrow \vec{0}$  ▷ Initialize
2: for each  $(\eta_t, \theta_{t-1}) \in \mathcal{P}$  do
3:    $\widehat{g}_{\text{te}} \leftarrow \nabla_{\theta} \mathcal{L}(\widehat{z}_{\text{te}}; \theta_{t-1})$ 
4:   for each  $z_i \in \mathcal{D}_{\text{tr}}$  do ▷ All examples
5:      $g_i \leftarrow \nabla_{\theta} \mathcal{L}(z_i; \theta_{t-1})$ 
6:     if calculating TracInCP then
7:        $\mathbf{v}_i \leftarrow \mathbf{v}_i + \frac{\eta_t}{b} \langle g_i, \widehat{g}_{\text{te}} \rangle$  ▷ Unnormalized (Sec. 3.2)
8:     else if calculating GAS then
9:        $\mathbf{v}_i \leftarrow \mathbf{v}_i + \frac{\eta_t}{b} \left\langle \frac{g_i}{\|g_i\|}, \frac{\widehat{g}_{\text{te}}}{\|\widehat{g}_{\text{te}}\|} \right\rangle$  ▷ Renormalized (Sec. 4.3)
10: return  $\mathbf{v}$ 
    
```

losses to be very low – so-called *group effects*. Generally, targeted attacks succeed by leveraging the group effect of adversarial set \mathcal{D}_{adv} on the target(s).

Definition 4.2. For influence estimator \mathcal{I} , the *renormalized influence*, $\widetilde{\mathcal{I}}$, replaces each gradient g in \mathcal{I} by its corresponding unit vector $\frac{g}{\|g\|}$.

We refer to this computation as *renormalization* since rescaling gradients removes the low-loss penalty. Renormalization places all training instances on equal footing and ensures that gradient and/or feature similarity is prioritized – not loss. Alternative renormalization schemes [4] are discussed in suppl. Section E.3.

Renormalized versions of Section 3.2’s static influence estimators are below. *Renormalized influence functions* in Eq. (8) does not include target gradient norm $\|\widehat{g}_{\text{te}}\|$ since it is a constant factor. For simplicity, Eq. (9)’s *renormalized representer point* uses signum function $\text{sgn}(\cdot)$ since for any scalar $u \neq 0$, $\text{sgn}(u) = \frac{u}{|u|}$, i.e., signum is equivalent to normalizing by magnitude.

$$\widetilde{\mathcal{I}}_{\text{IF}}(z_i, \widehat{z}_{\text{te}}) := \frac{1}{n} \nabla_{\theta} \mathcal{L}(\widehat{z}_{\text{te}}; \theta_T)^\top H_{\theta}^{-1} \left(\frac{\nabla_{\theta} \mathcal{L}(z_i; \theta_T)}{\|\nabla_{\theta} \mathcal{L}(z_i; \theta_T)\|} \right) \quad (8)$$

$$\widetilde{\mathcal{I}}_{\text{RP}}(z_i, \widehat{z}_{\text{te}}) := -\frac{1}{2\lambda n} \text{sgn} \left(\frac{\partial \mathcal{L}(z_i; \theta_T)}{\partial a_{y_i}} \right) \langle \mathbf{f}_i, \mathbf{f}_{\text{te}} \rangle \quad (9)$$

Renormalized versions of Section 3.2’s dynamic influence estimators appear below. Going forward, we refer to renormalized TracInCP (Eq. (11)) as *gradient aggregated similarity*, GAS, since it is essentially the weighted, gradient cosine similarity averaged across all of training. GAS’s procedure is detailed in Algorithm 1.⁸

$$\widetilde{\mathcal{I}}_{\text{TracIn}}(z_i, \widehat{z}_{\text{te}}) := \sum_{z_i \in \mathcal{B}_t} \frac{\eta_t}{b} \frac{\langle \nabla_{\theta} \mathcal{L}(z_i; \theta_{t-1}), \nabla_{\theta} \mathcal{L}(\widehat{z}_{\text{te}}; \theta_{t-1}) \rangle}{\|\nabla_{\theta} \mathcal{L}(z_i; \theta_{t-1})\| \|\nabla_{\theta} \mathcal{L}(\widehat{z}_{\text{te}}; \theta_{t-1})\|} \quad (10)$$

$$\begin{aligned} \widetilde{\mathcal{I}}_{\text{TracInCP}}(z_i, \widehat{z}_{\text{te}}) &:= \sum_{t \in \mathcal{T}} \frac{\eta_t}{b} \frac{\langle \nabla_{\theta} \mathcal{L}(z_i; \theta_{t-1}), \nabla_{\theta} \mathcal{L}(\widehat{z}_{\text{te}}; \theta_{t-1}) \rangle}{\|\nabla_{\theta} \mathcal{L}(z_i; \theta_{t-1})\| \|\nabla_{\theta} \mathcal{L}(\widehat{z}_{\text{te}}; \theta_{t-1})\|} \\ &=: \text{GAS}(z_i, \widehat{z}_{\text{te}}) \end{aligned} \quad (11)$$

⁸As shown in Algorithm 1, TracInCP’s procedure (Line 7) is identical to GAS (Line 10) other than influence renormalization.

Unlike static estimators, rescaling dynamic influence by target gradient norm $\|\widehat{g}_{\text{te}}\|$ is quite important as mentioned earlier. Intuitively, $\|\widehat{z}_{\text{te}}\|$ tends to be largest in two cases: (1) early in training due to initial parameter randomness and (2) when iteration t ’s predicted label conflicts with final label \widehat{y}_{te} . Both cases are consistent with the features most responsible for predicting \widehat{y}_{te} not yet dominating. Therefore, rescaling dynamic influence by $\|\widehat{g}_{\text{te}}\|$ implicitly upweights iterations where \widehat{y}_{te} is predicted confidently. It also inhibits any single checkpoint dominating the estimate.

Applying Renormalization to CIFAR10 & MNIST Joint Classification: Figure 1’s lower half demonstrates renormalization’s significant performance advantage over standard influence estimation – with the improvement in AUPRC as large as 25×. In particular, our renormalized estimators’ top-5 highest-ranked instances were all consistently from MNIST, unlike any of the standard influence estimators. Overall, GAS (renormalized TracInCP) was the top performer – even outperforming our other renormalized estimators by a wide margin.

4.4 Renormalization & More Advanced Attacks

Section 4.2 illustrates why influence performs poorly under a naive backdoor-style attack where the adversary does not optimize the adversarial set. Those concepts also generalize to more sophisticated attacks. For example, recent work shows that deep networks often predict the adversarial set with especially high confidence (i.e., low loss) due to shortcut learning – even on advanced attacks [21, 75]. Those findings reinforce the need for renormalization.

Dynamic methods – both TracIn and GAS – outperformed static ones for Section 4.1’s naive attack. The same can be expected for sophisticated attacks such as those that track the adversarial set’s gradients through simulated training [27, 68]. For such attacks, adversaries can craft \mathcal{D}_{adv} to exhibit particular gradient signatures at the end of training to avoid static detection. Moreover, models learn adversarial data faster than clean data meaning training loss often drops abruptly and significantly early in training [39]. For an attack to succeed, the adversarial instances must align with the target at some point during training, meaning dynamic methods can detect them.

Lastly, the threat model specifies that attackers never know the random batch sequence nor any randomly initialized parameters. Therefore, attackers can only craft \mathcal{D}_{adv} to be *influential in expectation* over that randomness. Influence is stochastic, varying significantly across random seeds. However, estimating the true expected influence is computationally expensive. GAS and TracInCP, which simulate expectation, better align with how the adversary actually crafts the adversarial set, resulting in better \mathcal{D}_{adv} identification.

Below we detail how renormalization can be specialized further for better adversarial-set identification.

Extending Renormalization Layerwise: In practice, gradient magnitudes are often unevenly distributed across a neural network’s layers. For example, Figure 3 tracks the target’s average intra-training gradient magnitude for two different backdoor adversarial triggers on CIFAR10 binary classification ($y_{\text{targ}} = \text{airplane}$

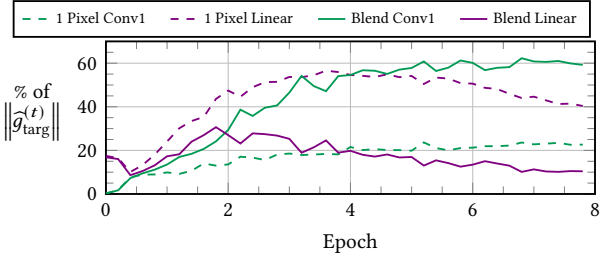


Figure 3: Layerwise Decomposition of a Target’s Intra-Training Gradient Magnitude: One-pixel & blend back-door adversarial triggers (dashed & solid lines respectively) trained separately on CIFAR10 binary classification ($y_{\text{targ}} = \text{airplane}$ & $y_{\text{adv}} = \text{bird}$) using ResNet9. The network’s first convolutional (Conv1) and final linear layers are a small fraction of the parameters (0.03% & 0.01% resp.) but constitute most of the target’s gradient magnitude ($\|\hat{g}_{\text{targ}}\|$) with the dominant layer attack dependent. Results are averaged over 20 trials.

and $y_{\text{adv}} = \text{bird}$).⁹ Specifically, Figure 3 decomposes target gradient norm, $\|\nabla_{\theta} \mathcal{L}(\hat{z}_{\text{targ}}; \theta_t)\|$, into just the contributions of the network’s first convolutional layer (Conv1) and the final linear layer. Despite being only 0.04% of the model’s parameters, these two layers combined constitute $>50\%$ of the gradient norm. Therefore, the first and last layers’ parameters are, on average, weighted $>2,000\times$ more than other layers’ parameters. With simple renormalization, important parameters in those other layers may go undetected.

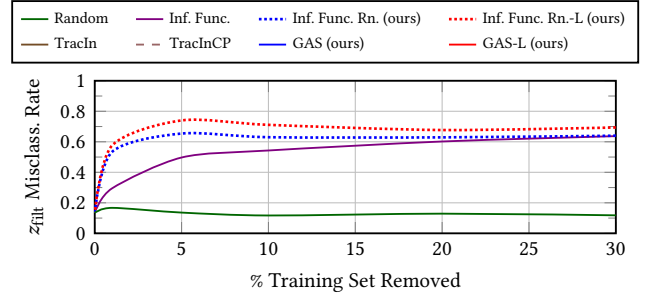
As an alternative to simply renormalizing by $\|\nabla_{\theta} \mathcal{L}(z; \theta_t)\|$, partition gradient vector g by layer into L disjoint vectors (where L is model f ’s layer count) and then independently renormalize each subvector separately. This *layerwise renormalization* can be applied to any estimator that uses training gradient g_i or test gradient \hat{g}_{te} , including influence functions, TracIn, and TracInCP. Layerwise renormalization still corrects for the low-loss penalty and does not change the asymptotic complexity. To switch GAS to layerwise, the only modification to Algorithm 1 is on Line 10 where each dimension is divided by its corresponding layer’s norm instead of the full gradient norm.

Additional inductive biases can be built into layerwise normalization by treating multiple layers as a single one similar to neural group normalization [71], but that is beyond this work’s scope.

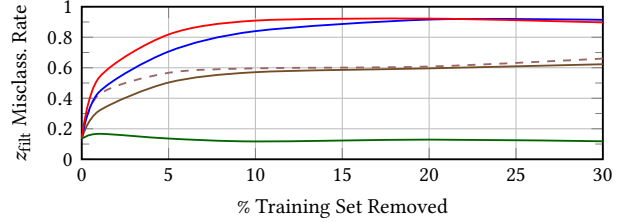
Notation: “-L” denotes layerwise renormalization, e.g., *layerwise* GAS is GAS-L. Suffix “(-L)”, e.g., GAS(-L), signifies that a statement applies irrespective of whether the renormalization is layerwise.

4.5 Renormalization & Non-Adversarial Data

Renormalization not only improves performance identifying an inserted adversarial set; it also improves performance in *non-adversarial* settings. Sec. 3.2 defines influence w.r.t. a single training example. Just as one instance may be more influential on a prediction than another, a group of training instances may be more influential



(a) Influence functions-based methods



(b) TracIn-based methods

Figure 4: Effect of Removing Influential, Non-Adversarial Training Data: Test example z_{filt} ’s misclassification rate (larger is better) when filtering the training set using influence rankings based on influence functions (top) and TracIn (bottom). Renormalization (Rn.) always improved mean performance across all training-set filtering percentages. Results are averaged across five CIFAR10 class pairs with 30 trials per class pair and 20 models trained per method per trial. Results are separated by the reference influence estimator.

than a different group. Renormalization improves identification of influential groups of examples, even on non-adversarial data.

To empirically demonstrate this, consider CIFAR10 binary classification again. In each trial, ResNet9 was pre-trained on eight ($= 10 - 2$) held-out CIFAR10 classes. From the other two classes, test example z_{filt} was selected u.a.r. from those instances with a moderate misclassification rate (10-20%) across multiple retrainings (i.e., fine-tunings) of the pre-trained network.¹⁰ (Renormalized) influence was then calculated for z_{filt} , with each metric yielding a training-set ranking. Each metric’s top $p\%$ ranked instances were removed from the training set and 20 models trained from the pre-trained parameters using these reduced training sets. Performance is measured using z_{filt} ’s misclassification rate across those 20 models where a larger error rate entails a better overall ranking.

Figure 4 compares influence estimation’s filtering performance, with and without renormalization, against a random baseline averaged across five CIFAR10 class pairs, namely the two pairs specified by Weber et al. [70] and three additional random pairs. Influence, irrespective of renormalization, significantly outperformed random removal, meaning all of these methods found influential subsets, albeit of varying quality.¹¹ In all cases, renormalized influence had

⁹See supplemental Section C for the complete experimental setup. The class pair and adversarial triggers were proposed by Weber et al. [70].

¹⁰Using examples with a moderate misclassification rate ensures that dataset filtering’s effects are measurable even with a small filtering percentage.

¹¹Representer point (Eq. (2)) is excluded as it underperformed random filtering.

better or equivalent performance to the original estimator across all filtering fractions. This demonstrates that renormalization generalizes across estimators even with no adversarial data.

Overall, layerwise renormalization was the top performer across all setups except for large filtering percentages where GAS surpassed it slightly. Renormalized(-L) Influence functions and GAS(-L) performed similarly when filtering a small fraction (e.g., $\leq 5\%$) of the training data. However, the performance of renormalized influence functions plateaued for larger filtering fractions ($\geq 10\%$) while GAS(-L)’s performance continued to improve. In addition, renormalization’s performance advantage for influence functions narrowed at larger filtering fractions. In contrast, GAS(-L)’s advantage over TracIn and TracInCP remained consistent. Recall that dynamic methods (e.g., GAS(-L) and TracIn) use significantly more gradient information than static methods (e.g., influence functions). This experiment again demonstrates that loss-based renormalization’s benefits increase as more gradient information is used.

5 IDENTIFYING ATTACK TARGETS

Recall that non-targets have primarily weak influences and few very strong ones. Target instances are outliers as they have an unusual number of highly-influential training instances. This idea serves as the core idea of our *framework for identifying targets* of training-set attacks, FIT. Algorithm 2 formalizes FIT as an end-to-end procedure to identify any targets in test example analysis set $\hat{\mathcal{Z}}_{te}$.¹² Overall, FIT has three sub-steps, described chronologically:

- (1) INF: Calculates (renormalized) influence vector \mathbf{v} for each test instance in analysis set $\hat{\mathcal{Z}}_{te}$.
- (2) ANOMSCORE: Targets have an unusual number of highly-influential instances. This step analyzes each testinstance’s influence vector \mathbf{v} and ranks those instances based on how anomalous their influence values are.
- (3) MITIGATE: Target-driven mitigation sanitizes model parameters θ_T and training set \mathcal{D}_{tr} to remove the attack’s influence on the most likely target \hat{z}_{targ} (e.g., the most anomalous misclassified instance). Alternatively, if human expertise is available, then a user can inspect the top-ranked candidates to choose any targets of interest and run target-driven mitigation on a manually-filtered target set $\hat{\mathcal{Z}}_{targ}$.

FIT is referred to as a “framework” since these subroutines are general and their underlying algorithms can change as new versions are developed. The next three subsections describe our implementation of each of these methods. For reference, Suppl. Alg. 6 specializes Alg. 2 to more closely align with the implementation details below.

5.1 Measuring (Renormalized) Influence

Algorithm 2 is agnostic of the specific (renormalized) influence estimator used to calculate \mathbf{v} , provided that method is sufficiently adept at identifying adversarial set \mathcal{D}_{adv} . We use GAS(-L) for the reasons explained in Section 4.4 as well as its simplicity, computational efficiency, and strong, consistent empirical performance.

¹²For simplicity, Alg. 2 considers a single identified target. If there are multiple identified targets, MITIGATE is invoked on each target serially with parameters $\tilde{\theta}_T$ and $\tilde{\mathcal{D}}_{tr}$.

Algorithm 2 FIT target identification & mitigation

Input: Training set \mathcal{D}_{tr} , test example set $\hat{\mathcal{Z}}_{te}$, and final params. θ_T
Output: Sanitized model parameters $\tilde{\theta}_T$ & training set $\tilde{\mathcal{D}}_{tr}$

- 1: $\mathcal{V} \leftarrow \{\text{INF}(\hat{z}; \mathcal{D}_{tr}) : \hat{z} \in \hat{\mathcal{Z}}_{te}\} \triangleright$ (Renorm.) Inf. (Alg. 1)
- 2: $\Sigma \leftarrow \{\text{ANOMSCORE}(\mathbf{v}, \mathcal{V}) : \mathbf{v} \in \mathcal{V}\} \triangleright$ Anomaly score (Sec. 5.2)
- 3: Rank $\hat{\mathcal{Z}}_{te}$ by anomaly scores Σ
- 4: $\hat{z}_{targ} \leftarrow$ Most anomalous test example in $\hat{\mathcal{Z}}_{te}$
- 5: $\tilde{\theta}_T, \tilde{\mathcal{D}}_{tr} \leftarrow \text{MITIGATE}(\hat{z}_{targ}, \theta_T, \mathcal{D}_{tr}) \triangleright$ Sec. 5.3
- 6: **return** $\tilde{\theta}_T, \tilde{\mathcal{D}}_{tr}$

Time and Space Complexity: Computing a gradient requires $O(|\theta|)$ time and space. For fixed T and $|\theta|$, TracInCP, GAS, and GAS-L require $O(n)$ time and space to calculate each test instance’s influence vector \mathbf{v} . The next section explains that FIT analyzes each test instance’s influence vector \mathbf{v} meaning GAS(-L) can be significantly sped-up by amortizing training gradient ($g_i^{(t)}$) computation across multiple test examples – either on a single node (Sec. E.5) or across multiple nodes (e.g., using all-reduce).

5.2 Identifying Anomalous Influence

To change a prediction, adversarial set \mathcal{D}_{adv} must be highly influential on the target. When visualizing \hat{z}_{te} ’s influence vector \mathbf{v} as a density distribution, an exceptionally influential \mathcal{D}_{adv} manifests as a distinct density mass at the distribution’s positive extreme.

Figures 5a and 5d each plot an attack target’s GAS influence as a density for two different training-set attacks – the first poisoning on vision [77] and the other a backdoor attack on speech recognition [43]. For both attacks, adversarial set \mathcal{D}_{adv} ’s influence significantly exceeds that of \mathcal{D}_{cl} . When compared to theoretical normal (calculated¹³ w.r.t. complete training set \mathcal{D}_{tr}), \mathcal{D}_{adv} ’s target influence is highly anomalous. In Figures 5b and 5e, which plot the GAS influence of non-targets for the same two attacks, no extremely high influence instances are present.

Going forward, influence vectors \mathbf{v} with exceptionally high influence instances are referred to as having a *heavy upper-tail*. Then, *target identification simplifies to identifying influence vectors whose values have anomalously heavy upper-tails*. The preceding insight is relative and is w.r.t. to other test instances’ influence value distributions. Non-target baseline anomaly quantities vary with model, dataset, and hyperparameters. That is why Algorithm 6 ranks candidates in $\hat{\mathcal{Z}}_{te}$ based on their upper-tail heaviness.

Quantifying Tail Heaviness: Determining whether \hat{z}_{te} ’s influence vector \mathbf{v} is abnormal simplifies to univariate anomaly detection for which significant previous work exists [3, 26, 56, 57]. Observe in Figures 5b and 5e that \mathcal{D}_{cl} ’s GAS influence vector \mathbf{v} tends to be normally distributed (see the close alignment to the dashed line). We therefore use the traditional *anomaly score*, $\sigma := \frac{\mathbf{v} - \mu}{s}$, where μ and s are each \mathbf{v} ’s center and dispersion statistics, resp.¹⁴ Mean and standard deviation, the traditional center and dispersion statistics, resp., are not robust to outliers. Both have an asymptotic *breakdown*

¹³The plotted theoretical normal used robust statistics median and Q in place of mean and standard deviation.

¹⁴In Algorithm 6, statistics $\mu^{(j)}$ and $Q^{(j)}$ are calculated separately for each test instance \hat{z}_j ’s influence vector $\mathbf{v}^{(j)}$.

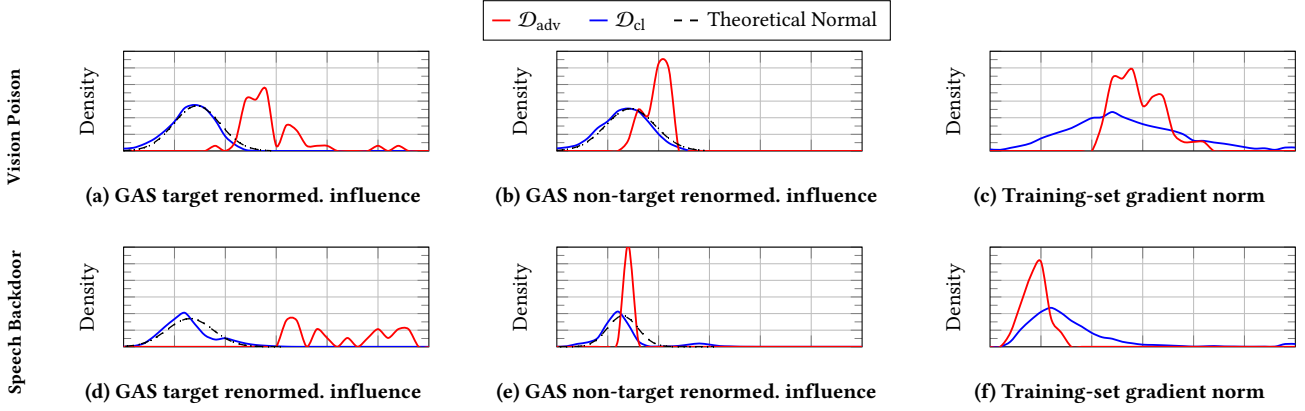


Figure 5: GAS renormalized influence, v , density distributions for two training-set attacks: CIFAR10 vision poisoning [77] ($y_{\text{target}} = \text{dog}$ & $y_{\text{adv}} = \text{bird}$) & speech-recognition backdoor [43] ($y_{\text{target}} = 4$ & $y_{\text{adv}} = 5$). Theoretical normal (—) is w.r.t. $\mathcal{D}_{\text{tr}} := \mathcal{D}_{\text{adv}} \cup \mathcal{D}_{\text{tr}}$. Observe that target examples (Figs. 5a & 5d) have significant \mathcal{D}_{adv} mass (—) well to the right of \mathcal{D}_{cl} ’s mass (—). This upper-mass phenomenon is absent in non-targets (Figs. 5b & 5e). Training example gradient norms (Fig. 5c & 5f) are poorly correlated with whether the training example is adversarial. For example, speech recognition has \mathcal{D}_{cl} mass well to the right of even the right-most \mathcal{D}_{adv} mass, necessitating renormalization. See Sections 6.1 and C for more details on these attacks.

point of 0 (one anomaly can shift the estimator arbitrarily). Since \mathcal{D}_{adv} instances are inherently outliers, robust statistics are required.

Median serves as our center statistic μ given its optimal breakdown (50%). Although median absolute deviation (MAD) is the best known robust dispersion statistic, we use Rousseeuw and Croux’s [55] Q estimator, which retains MAD’s benefits while addressing its weaknesses. Specifically, both MAD and Q have optimal breakdowns, but Q has better Gaussian data efficiency (82% vs. 37%). Critically for our setting with one-sided anomalies, Q does not assume data symmetry – unlike MAD. Formally,

$$Q := c\{|\mathbf{v}_i - \mathbf{v}_l| : 1 \leq i < l \leq n\}_{(r)}, \quad (12)$$

where $\{\cdot\}_{(r)}$ denotes the set’s r -th order statistic with $r = (\lfloor \frac{n}{2} \rfloor + 1)$ and c is a distribution consistency constant which for Gaussian data, $c \approx 2.2219$ [56]. Eq. (12) requires only $\mathcal{O}(n)$ space and $\mathcal{O}(n \lg n)$ time as proved by Croux and Rousseeuw [13]. Provided anomaly score vector σ , upper-tail heaviness is simply $\sigma_{(n-\kappa)}$, which is σ ’s $(n - \kappa)$ th order statistic, i.e., \hat{z}_{te} ’s κ th largest anomaly score value.

Multiclass vs. Binary Classification Different classes are implicitly generated from different data distributions. Each class’s data distribution may have different influence tails – in particular in multiclass settings. Target identification performance generally improves (1) when μ and Q are calculated w.r.t. only training instances labeled \hat{y}_{te} and (2) \hat{z}_{te} ’s upper-tail heaviness is ranked w.r.t. other test instances labeled \hat{y}_{te} .

Faster FIT The execution time of TracInCP and by extension GAS(-L), depends on parameter count $|\theta|$. For very large models, target identification can be significantly sped up via a two-phase strategy. In phase 1, GAS(-L) uses a very small iteration subset (e.g., $\mathcal{T} = \{T\}$) to coarsely rank analysis set \hat{z}_{te} . Phase 2 then uses the complete \mathcal{T} but only on a small fraction (e.g., 10%) of \hat{z}_{te} with the heaviest phase 1 tails. Section 6.3 applies this approach to natural-language data poisoning on RoBERTaBASE [44].

Computing each test instance’s ($\hat{z}_{\text{te}} \in \hat{Z}_{\text{te}}$) influence vector \mathbf{v} is independent. Each dimension v_i is also independent and can be separately computed. Hence, GAS(-L) is embarrassingly parallel allowing linear speed-up of target identification via parallelization.

5.3 Target-Driven Attack Mitigation

A primary benefit of target identification is that attack mitigation becomes straightforward. Algorithm 3 mitigates attacks by sanitizing training set \mathcal{D}_{tr} of adversarial set \mathcal{D}_{adv} . Most importantly, target identification solves data sanitization’s common pitfall (Sec. 3.1) of determining how much data to remove. *Sanitization stops when the target’s misprediction is eliminated.* Therefore, successfully identifying a target means sanitization is *guaranteed to succeed tautologically* (i.e., attack success rate on any analyzed targets is 0).

More concretely, Alg. 3 iteratively filters \mathcal{D}_{tr} by thresholding anomaly score vector, σ .¹⁵ Since adversarial instances are abnormally influential on targets, Alg. 3 filters \mathcal{D}_{adv} instances first. After each iteration, influence is remeasured to account for estimation stochasticity and because training dynamics may change with different training sets. Data removal threshold ζ is tuned based on computational constraints – larger ζ results in less clean data removed but may take more iterations. Slowly annealing ζ also results in less clean-data removal.

Given forensic or human analysis of the identified target(s), simpler mitigation than Algorithm 3 is possible, e.g., a naive, rule-based, corrective lookup table that entails no clean data removal at all.

6 EVALUATION

We empirically demonstrate our method’s agnosticism by evaluating training-set attacks on different data modalities, including text classification, vision, and speech recognition. We consider both

¹⁵ Alg. 3 considers the more general case of a single identified target but can be extended to consider multiple targets. For instance, provided there is a single attack, average \mathbf{v} across all targets, and stop sanitizing once all targets are classified correctly.

Algorithm 3 Target-driven mitigation & sanitization

Input: Target $\hat{z}_{\text{target}} := (x_{\text{target}}, y_{\text{adv}})$, anomaly cutoff ζ , model f , initial params. θ_0 , final params. θ_T , and training set \mathcal{D}_{tr}

Output: Clean model params. $\tilde{\theta}_T$ & sanitized training set $\tilde{\mathcal{D}}_{\text{tr}}$

```

1: function MITIGATE( $\hat{z}_{\text{target}}, \theta_T, \mathcal{D}_{\text{tr}}$ )
2:    $\tilde{\theta}_T, \tilde{\mathcal{D}}_{\text{tr}} \leftarrow \theta_T, \mathcal{D}_{\text{tr}}$ 
3:   while  $\arg \max (f(x_{\text{target}}; \tilde{\theta}_T)) = y_{\text{adv}}$  do
4:      $\mathbf{v} \leftarrow \text{INF}(\hat{z}_{\text{target}}; \mathcal{D}_{\text{tr}})$             $\triangleright$  Renorm. Influence (Alg. 1)
5:      $\sigma \leftarrow \frac{\mathbf{v} - \mu}{Q}$                       $\triangleright$  Anomaly score (Sec. 5.2)
6:      $\tilde{\mathcal{D}}_{\text{tr}} \leftarrow \mathcal{D}_{\text{tr}} \setminus \{z_i : \sigma_i \geq \zeta \wedge z_i \in \mathcal{D}_{\text{tr}}\}$   $\triangleright$  Sanitize
7:      $\tilde{\theta}_T \leftarrow \text{RETRAIN}(\theta_0, \tilde{\mathcal{D}}_{\text{tr}})$ 
8:     Optionally anneal  $\zeta$ 
9:   return  $\tilde{\theta}_T, \tilde{\mathcal{D}}_{\text{tr}}$ 

```

data poisoning and backdoor attacks on pre-trained and randomly-initialized, state-of-the-art models in both binary and multiclass settings. Due to space, most evaluation setup details (e.g., model architectures) are deferred to supplemental Section C. Hyperparameter settings – for model training, our method, and the baselines – appear in Section C.2. Additional experimental results (e.g., hyperparameter sensitivity study, analysis of gradient aggregation’s benefits, execution times, etc.) also appear in the supplement.

6.1 Training-Set Attacks Evaluated

We evaluated our method on four published training-set attacks – two *single-target* data poisoning and two multi-target backdoor. Below are brief details regarding how each attack crafts adversarial set \mathcal{D}_{adv} , with the full details in suppl. Sec. C.2.4. Representative clean and adversarial training instances for each attack appear in suppl. Sec. D. Below, $y_{\text{target}} \rightarrow y_{\text{adv}}$ denotes the target’s true and adversarial labels, respectively. When an attack considers multiple class pairs or setups, each is evaluated separately.

(1) *Speech Backdoor*: Liu et al.’s [43] speech recognition dataset contains spectrograms of human speech pronouncing in English digits 0 to 9 (10 classes, $|\mathcal{D}_{\text{cl}}| = 3,000$). Liu et al. also provide 300 backdoored training instances evenly split between the 10 classes. Each class’s adversarial trigger – a short burst of white noise at the recording’s beginning – induces the spoken digit to be misclassified as the next largest digit (e.g., $0 \rightarrow 1$, $1 \rightarrow 2$, etc.). This small input-space signal induces a large feature-space perturbation – too large for most certified methods. Following Liu et al., our evaluation used a speech recognition CNN trained from scratch.

(2) *Vision Backdoor*: Weber et al. [70] consider three different backdoor adversarial trigger patterns on CIFAR10 binary classification. Specifically, Weber et al.’s “pixel” attack patterns increase the pixel value of either one or four central pixel(s) by a specified maximum ℓ_2 perturbation distance while their “blend” trigger pattern adds fixed $\mathcal{N}(0, I)$ Gaussian noise across all perturbed images. We considered the same class pairs as Weber et al. (auto \rightarrow dog and plane \rightarrow bird) on the state-of-the-art ResNet9 [47] CNN trained from scratch with $|\mathcal{D}_{\text{adv}}| = 150$ and $|\mathcal{D}_{\text{tr}}| = 10,000$.

(3) *Natural Language Poison*: Wallace et al. [68] construct text-based poison by simulating bilevel optimization via second-order

gradients. \mathcal{D}_{adv} ’s instances are crafted via iterative word-level substitution given a target phrase. We follow Wallace et al.’s [68] experimental setup of poisoning¹⁶ the Stanford Sentiment Treebank v2 (SST-2) sentiment analysis dataset [61] ($|\mathcal{D}_{\text{cl}}| = 67,349$ & $|\mathcal{D}_{\text{adv}}| = 50$) on RoBERTa_{BASE} (125M parameters) [44].

(4) *Vision Poison*: Zhu et al.’s [77] targeted, clean-label attack crafts poisons by forming a convex polytope around a single target’s feature representation. Following Zhu et al., the pre-train then fine-tune paradigm was used. In each trial, ResNet9 was pre-trained using half the classes (none were y_{target} or y_{adv}). Targets were selected u.a.r. from test examples labeled y_{target} , and 50 poison instances were then crafted from seed examples labeled y_{adv} . The pre-trained network was fine-tuned using \mathcal{D}_{adv} and the five held-out classes’ training data ($|\mathcal{D}_{\text{tr}}| = 25,000$). Like previous work [27, 60], CIFAR10 class pairs dog vs. bird and deer vs. frog were evaluated, where each class in a pair serves alternately as y_{target} and y_{adv} .

While it is not feasible to evaluate our approach on every attack – since new attacks are developed and published so frequently – we believe this diverse set of attacks is representative of training-set attacks in general and demonstrates the broad applicability of our approach. In particular, our methods are not tailored to these attacks but could be used against future attacks as well, as long as the attack includes a group of highly influential training examples that attack specific targets.

6.2 Identifying Adversarial Set \mathcal{D}_{adv}

To identify the target (Alg. 2) or mitigate the attack (Alg. 3), we must be able to identify the likely adversarial instances \mathcal{D}_{adv} associated with a possible target \hat{z}_{target} . Our approach is to use influence-estimation methods, which should rank an actual adversarial attack \mathcal{D}_{adv} as more influential than clean instances \mathcal{D}_{cl} on the target. In this section, we evaluate how well different influence-estimation methods succeed at performing this ranking for a given target.

We compare the performance of our renormalized estimators, GAS and GAS-L, against Section 3.2’s four influence estimators: TracInCP, TracIn, influence functions, and representer point. As an even stronger baseline, where applicable, we also compare against Peri et al.’s [50] Deep k -NN empirical training-set defense specifically designed for Zhu et al.’s [77]’s vision, clean-label poisoning attack; described briefly, Deep k -NN sanitizes the training set of instances whose nearest feature-space neighbors have a different label. Like Section 4’s CIFAR10 & MNIST joint classification experiment, class sizes are imbalanced ($|\mathcal{D}_{\text{adv}}| \ll |\mathcal{D}_{\text{cl}}|$) so performance is again measured using AUPRC.

For targets selected u.a.r., Figure 6 details each method’s averaged adversarial-set identification AUPRC for Section 6.1’s four attacks.¹⁷ In summary, GAS and GAS-L were each the top performer for one attack and had comparable performance for the other two.

GAS and GAS-L identified the adversarial instances nearly perfectly for Liu et al.’s speech backdoor and Wallace et al.’s text poisoning attacks. Standard influence estimation performed poorly on the text poisoning attack (in particular the static estimators) due to

¹⁶Wallace et al. [68] provided their original implementation via personal correspondence, and their implementation was used to craft the poison.

¹⁷Averaging provides a holistic performance overview. Supplemental Section E.1 provides a granular, numerical breakdown of each method’s performance (including variance) across classes and attack patterns.

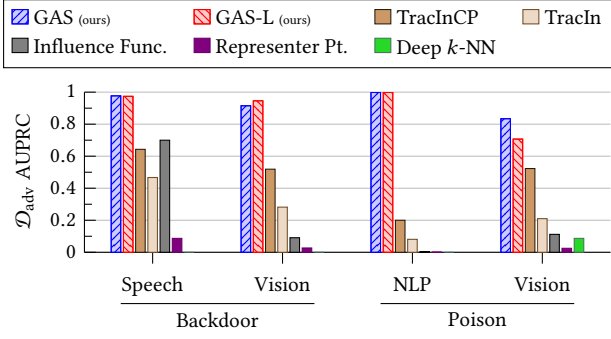


Figure 6: Adversarial-Set Identification: Mean AUPRC identifying adversarial set \mathcal{D}_{adv} using a randomly selected target for Sec. 6.1’s four attacks. Results averaged across related setups with ≥ 10 trials per setup. See supplemental Section E.1 for the full granular results including variance.

the large model, RoBERTa_{BASE}, that Wallace et al.’s attack considers. For the vision backdoor and poisoning attacks, our renormalized estimators successfully identified most of \mathcal{D}_{adv} – again, much better than the four original estimators. While Peri et al.’s [50] Deep k -NN defense can be effective at stopping clean-label vision poisoning, it does so by removing a comparatively large fraction of clean data (up to 4.3% on average) resulting in poor AUPRC.

For completeness, Figure 8 provides adversarial-set identification results for our renormalized, static influence estimators. In all cases, renormalization improved the influence estimator’s performance, generally by an order of magnitude with a maximum improvement of 600 \times . These experiments highlight layerwise renormalization’s benefits. Influence functions’ Hessian-vector product algorithm [49] can assign a large magnitude to some layers, and these layers then dominate the influence and GAS estimates. Layerwise renormalization addresses this, improving renormalized influence function’s adversarial-set identification AUPRC by up to 3.5 \times .

The only case where renormalization did not yield a large improvement over the original static estimator was representer point on vision poisoning. This is due to large variances in the poisoned model’s penultimate feature vector’s norm $\|f_i\|$ – an issue to which representer point is uniquely susceptible. When also normalizing for $\|f_i\|$, renormalized representer point’s mean AUPRC jumps to 0.881 – very close to GAS’s performance.

6.3 Identifying Attack Targets

The previous experiments demonstrate that knowledge of a target enables identification of the adversarial set when using renormalization. This section demonstrates that the distribution of renormalized influence values actually enables us to identify target(s) in the first place, through the interplay foundational to our target identification framework, FIT. Since target identification is a new task, we propose four target identification baselines. First, inspired by Peri et al.’s [50] Deep k -NN empirical defense, *maximum k -NN distance* computes the distance from each test instance to its κ^{th} nearest neighbor in the training data, as measured by the L_2 distance between their penultimate feature representations (f). It orders them

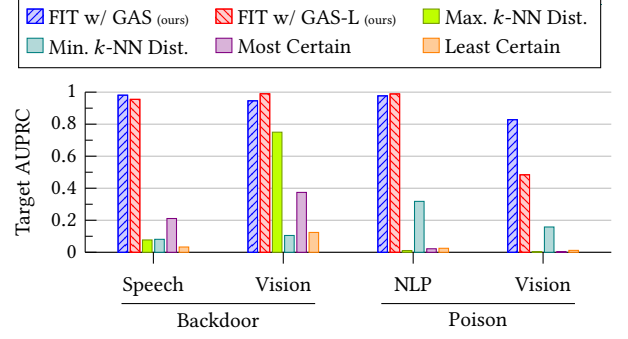


Figure 7: Target Identification: Mean target identification AUPRC for Sec. 6.1’s four attacks. “FIT w/ GAS” denotes GAS was FIT’s influence estimator with matching notation for GAS-L. Results averaged across setups with ≥ 10 trials per setup. See Sec. E.1 for the full granular results inc. variance.

by this distance, starting with the largest distance to the κ^{th} neighbor, thus prioritizing outliers and instances in sparse regions of the learned representation space. *Minimum k -NN distance* is the reverse ordering, prioritizing instances in dense regions. The other two baselines are *most certain*, which ranks test examples in ascending order by loss while *least certain* ranks by descending loss.

There are far fewer targets than possible test examples so performance is again measured using AUPRC. See suppl. Table 5 for the number of targets and non-targets analyzed for each attack. For single-target attacks (vision and natural language poisoning), target identification AUPRC is equivalent to the target’s inverse rank, causing AUPRC to decline geometrically.

Figure 7 shows that FIT – using either GAS or GAS-L as the influence estimator – achieves near-perfect target identification for both backdoor attacks and natural language poisoning. Overall, FIT with GAS was the top performer on two attacks, and FIT with GAS-L was the best for the other two. Recall that the vision poisoning attack is single target. Hence, GAS-based FIT’s mean AUPRC of > 0.8 equates to an average target rank better than 1.25 ($1/0.8$), i.e., three out of four times on average \hat{z}_{targ} was the top-ranked – also very strong target detection. FIT’s performance degradation on vision poisoning is due to GAS and GAS-L identifying this attack’s \mathcal{D}_{adv} slightly worse (Fig. 6). Only maximum k -NN approached FIT’s performance – specifically for Weber et al.’s vision backdoor attack. Note also that no baseline consistently outperformed the others. Hence, these attacks affect network behavior differently, further supporting that FIT is attack agnostic.

Suppl. Sec. E.2 shows that FIT’s performance is stable across a wide range of upper-tail cutoff thresholds κ . For example, FIT’s natural language target identification AUPRC varied only 0.2% and 2.1% when using GAS-L and GAS respectively for $\kappa \in [1, 25]$; their vision backdoor target identification AUPRC varied only 1.8% and 5.8% respectively for $\kappa \in [2, 50]$.

6.4 Target-Driven Mitigation

Section 5.3 explains that successfully identifying the target(s) enables guaranteed attack mitigation on those instances. Here, we

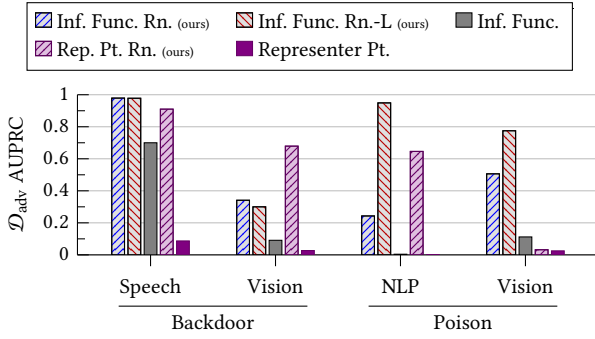


Figure 8: Static Influence Adversarial-Set Identification: Comparing the mean adversarial-set identification AUPRC of the static influence estimators and their corresponding renormalized (Rn.) versions. For all attacks, renormalization improved the static estimators’ mean performance by up to a factor of $>600\times$. These experiments also highlight layerwise renormalization’s performance gains, e.g., influence func. on natural language poison. Results are averaged across related experimental setups with ≥ 10 trials per setup.

evaluate GAS and GAS-L’s effectiveness in targeted data sanitization. Table 1 details our defense’s effectiveness against Sec. 6.1’s four attacks. As above, results are averaged across each attack’s class pairs/setup. Section 6’s baselines all have large false-positive rates when identifying \mathcal{D}_{adv} (Fig. 6), which caused them to remove a large fraction of \mathcal{D}_{cl} and are not reported in these results.

For three of four attacks, clean test accuracy after sanitization either improved or stayed the same. In the case of Weber et al.’s vision backdoor attack, the performance degradation was very small – 0.1%. Similarly, owing to renormalized influence’s effectiveness identifying \mathcal{D}_{adv} (Fig. 7), our defense removes very little clean data when mitigating the attack – generally $<0.2\%$ of the clean training set. For comparison, Peri et al. [50] report that their Deep k -NN clean-label, poisoning defense removes on average 4.3% of \mathcal{D}_{cl} on Zhu et al.’s [77] vision poisoning attack. This is despite Peri et al.’s method being specifically tuned for Zhu et al.’s attack and their evaluation setup being both easier and less realistic by pre-training their model using a large known-clean set that is identically distributed to their \mathcal{D}_{cl} . In contrast, target-driven mitigation removed at most 0.03% of clean data on this attack – better than them by two orders of magnitude.

Following Algorithm 3, Table 1’s experiments used only a single, randomly-selected target when performing sanitization. No steps were taken to account for additional potential targets, e.g., over-filtering the training set. Nonetheless, target-driven mitigation still significantly degraded multi-target attacks’ performance on other targets not considered when sanitizing. For example, despite considering one target, speech backdoor’s overall attack success rate (ASR) across all targets decreased from 100% to 4.7% and 6.5% for GAS and GAS-L, respectively – a $20\times$ reduction. For Weber et al.’s vision backdoor attack, ASR dropped from 90.5% to 11.9% and 6.7% with GAS and GAS-L, respectively. The *key takeaway* is that identifying a single target almost entirely mitigates the attack everywhere.

Table 1: Target-Driven Attack Mitigation: Algorithm 3’s target-driven, iterative data sanitization applied to Section 6.1’s four attacks for randomly selected targets. The attacks were neutralized with few clean instances removed and little change in test accuracy. Attack success rate (ASR) is w.r.t. specifically the analyzed target. Results are averaged across related experimental setups with ≥ 10 trials per setup.

	Dataset	Method	% Removed		ASR %		Test Acc. %	
			\mathcal{D}_{adv}	\mathcal{D}_{cl}	Orig.	Ours	Orig.	Chg.
Backdoor	Speech	GAS	98.4	0.07	99.8	0	97.7	0.0
		GAS-L	98.1	0.17	99.8	0	97.7	0.0
	Vision	GAS	87.6	0.50	90.5	0	96.2	-0.1
		GAS-L	92.3	0.73	90.5	0	96.2	-0.1
Poison	NLP	GAS	99.6	0.02	97.9	0	94.2	+0.2
		GAS-L	99.9	0.03	97.9	0	94.2	+0.1
	Vision	GAS	65.1	0.02	77.9	0	87.1	0.0
		GAS-L	58.6	0.03	77.9	0	87.1	0.0

7 DISCUSSION AND CONCLUSIONS

This paper explores two related tasks. First, we propose training-set attack *target identification*. This task is an important part of protecting critical ML systems but has thus far received relatively little attention. For example, it is impossible to conduct a truly informed cost-benefit analysis of risk without knowing the attacker’s target and by extension their objective. Knowledge of the target also enables forensic and security analysts to reason about an attacker’s identity – a key step to permanently stopping attacks by disabling the attacker. An open question is whether target identification can be combined with certified guarantees, either building on our FIT framework or creating an alternative to it.

FIT relies on identifying (groups of) highly influential training instances. To that end, we propose *renormalized influence*. By addressing influence’s low-loss penalty, renormalization significantly improves influence estimation in both adversarial and non-adversarial settings – often by an order of magnitude or more. Renormalization’s consistently strong performance is surprising (to us), and it merits future work to fully understand the trade-offs, including determining the class of problems where standard influence estimation may be preferable.

ACKNOWLEDGMENTS

The authors would like to thank Jonathan Brophy for helpful discussions and feedback.

This work was supported by a grant from the Air Force Research Laboratory and the Defense Advanced Research Projects Agency (DARPA) – agreement number FA8750-16-C-0166, subcontract K001892-00-S05, as well as a second grant from DARPA, agreement number HR00112090135. This work benefited from access to the University of Oregon high performance computer, Talapas.

REFERENCES

- [1] Shruti Agarwal, Hany Farid, Yuming Gu, Mingming He, Koki Nagano, and Hao Li. 2019. Protecting World Leaders Against Deep Fakes. In *Proceedings of the CVPR Workshop on Media Forensics*. Long Beach, California.
- [2] Hojjat Aghakhani, Thorsten Eisenhofer, Lea Schönherr, Dorothea Kolossa, Thorsten Holz, Christopher Kruegel, and Giovanni Vigna. 2020. VENO-MAVE: Clean-Label Poisoning Against Speech Recognition. *CoRR* (2020). arXiv:cs.SD/2010.10682
- [3] Vic Barnett and Toby Lewis. 1978. *Outliers in Statistical Data* (2nd edition ed.). John Wiley & Sons Ltd., Hoboken, New Jersey, USA.
- [4] Elnaz Barshan, Marc-Etienne Brunet, and Gintare Karolina Dziugaite. 2020. RelatIF: Identifying Explanatory Training Samples via Relative Influence. In *Proceedings of the 23rd International Conference on Artificial Intelligence and Statistics (AISTATS’20)*.
- [5] Samyadeep Basu, Phil Pope, and Soheil Feizi. 2021. Influence Functions in Deep Learning Are Fragile. In *Proceedings of the 9th International Conference on Learning Representations (ICLR’21)*. Virtual Only.
- [6] Samyadeep Basu, Xuchen You, and Soheil Feizi. 2020. On Second-Order Group Influence Functions for Black-Box Predictions. In *Proceedings of the 37th International Conference on Machine Learning (ICML’20)*. PMLR, Virtual Only.
- [7] Battista Biggio, Blaine Nelson, and Pavel Laskov. 2012. Poisoning Attacks against Support Vector Machines. In *Proceedings of the 29th International Conference on Machine Learning (ICML’12)*. PMLR, Edinburgh, Great Britain.
- [8] Jonathan Brophy and Daniel Lowd. 2020. TREX: Tree-Ensemble Representer-Point Explanations. In *Proceedings of the ICMML Workshop on Extending Explainable AI Beyond Deep Models and Classifiers (XXAI)*.
- [9] Bryant Chen, Wilka Carvalho, Nathalie Baracaldo, Heiko Ludwig, Benjamin Edwards, Taesung Lee, Ian Molloy, and Biprav Srivastava. 2019. Detecting Backdoor Attacks on Deep Neural Networks by Activation Clustering. In *Proceedings of the AAAI Workshop on Artificial Intelligence Safety (SafeAI’19)*. Association for the Advancement of Artificial Intelligence, Honolulu, Hawaii, USA.
- [10] Xinyun Chen, Chang Liu, Bo Li, Kimberly Lu, and Dawn Song. 2017. Targeted Backdoor Attacks on Deep Learning Systems Using Data Poisoning. (2017). arXiv:cs.CR/1712.05526
- [11] Yuanyuan Chen, Boyang Li, Han Yu, Pengcheng Wu, and Chunyan Miao. 2021. HyDRA: Hypergradient Data Relevance Analysis for Interpreting Deep Neural Networks. In *Proceedings of the 35th AAAI Conference on Artificial Intelligence (AAAI’21)*. Association for the Advancement of Artificial Intelligence, Virtual Only.
- [12] Cody A. Coleman, Deepak Narayanan, Daniel Kang, Tian Zhao, Jian Zhang, Luigi Nardi, Peter Bailis, Kunle Olukotun, Chris Ré, and Matei Zaharia. 2017. DAWNbench: An End-to-End Deep Learning Benchmark and Competition. In *Proceedings of the 2017 NeurIPS Workshop on Machine Learning Systems*. Curran Associates, Inc., Long Beach, California, USA.
- [13] Christophe Croux and Peter J. Rousseeuw. 1992. A Class of High-Breakdown Scale Estimators Based on Subranges. *Communications in Statistics - Theory and Methods* 21, 7 (1992), 1935–1951.
- [14] Jesse Davis and Mark Goadrich. 2006. The Relationship Between Precision-Recall and ROC Curves. In *Proceedings of the 23rd International Conference on Machine Learning (ICML’06)*. PMLR, Pittsburgh, Pennsylvania.
- [15] Bao Gia Doan, Ehsan Abbasnejad, and Damith C. Ranasinghe. 2020. Februus: Input Purification Defense Against Trojan Attacks on Deep Neural Network Systems. In *Proceedings of the 36th Annual Computer Security Applications Conference (ACSAC’2020)*. Association for Computing Machinery, Virtual Only.
- [16] Vitaly Feldman and Chiyuan Zhang. 2020. What Neural Networks Memorize and Why: Discovering the Long Tail via Influence Estimation. In *Proceedings of the 34th Conference on Neural Information Processing Systems (NeurIPS’20)*. Curran Associates, Inc., Virtual Only.
- [17] Chelsea Finn, Pieter Abbeel, and Sergey Levine. 2017. Model-Agnostic Meta-Learning for Fast Adaptation of Deep Networks. In *Proceedings of the 34th International Conference on Machine Learning (ICML’17)*. PMLR, Sydney, Australia.
- [18] Liam Fowl, Micah Goldblum, Ping-yeh Chiang, Jonas Geiping, Wojtek Czaja, and Tom Goldstein. 2021. Adversarial Examples Make Strong Poisons. In *Proceedings of the 35th Conference on Neural Information Processing Systems (NeurIPS’21)*. Curran Associates, Inc., Virtual Only.
- [19] Yansong Gao, Change Xu, Derui Wang, Shiping Chen, Damith C. Ranasinghe, and Surya Nepal. 2019. STRIP: A Defence against Trojan Attacks on Deep Neural Networks. In *Proceedings of the 35th Annual Computer Security Applications Conference (ACSAC’19)*. Association for Computing Machinery, San Juan, Puerto Rico, USA.
- [20] Jonas Geiping, Liam Fowl, W. Ronny Huang, Wojciech Czaja, Gavin Taylor, Michael Moeller, and Tom Goldstein. 2021. Witches’ Brew: Industrial Scale Data Poisoning via Gradient Matching. In *Proceedings of the 9th International Conference on Learning Representations (ICLR’21)*. Virtual Only.
- [21] Robert Geirhos, Jörn-Henrik Jacobsen, Claudio Michaelis, Richard Zemel, Wieland Brendel, Matthias Bethge, and Felix A. Wichmann. 2020. Shortcut Learning in Deep Neural Networks. *Nature Machine Intelligence* 2, 11 (2020), 665–673.
- [22] Tianyu Gu, Kang Liu, Brendan Dolan-Gavitt, and Siddharth Garg. 2019. BadNets: Evaluating Backdoor Attacks on Deep Neural Networks. *IEEE Access* 7 (2019), 47230–47244.
- [23] Han Guo, Nazneen Fatema Rajani, Peter Hase, Mohit Bansal, and Caiming Xiong. 2020. FastIF: Scalable Influence Functions for Efficient Model Interpretation and Debugging. *CoRR* abs/2012.15781 (2020). arXiv:2012.15781 <http://arxiv.org/abs/2012.15781>
- [24] Zayd Hammoudeh and Daniel Lowd. 2021. Simple, Attack-Agnostic Defense Against Targeted Training Set Attacks Using Cosine Similarity. In *Proceedings of the 3rd ICML Workshop on Uncertainty and Robustness in Deep Learning (UDL’21)*.
- [25] Satoshi Hara, Atsushi Nitanda, and Takanori Maehara. 2019. Data Cleansing for Models Trained with SGD. In *Proceedings of the 33rd Conference on Neural Information Processing Systems (NeurIPS’19)*. Curran Associates, Inc., Vancouver, Canada.
- [26] Victoria J. Hodge and Jim Austin. 2004. A Survey of Outlier Detection Methodologies. *Artificial Intelligence Review* 22, 2 (Oct 2004), 85–126.
- [27] W. Ronny Huang, Jonas Geiping, Liam Fowl, Gavin Taylor, and Tom Goldstein. 2020. MetaPoison: Practical General-purpose Clean-label Data Poisoning. In *Proceedings of the 34th Conference on Neural Information Processing Systems (NeurIPS’20)*. Curran Associates, Inc., Virtual Only.
- [28] Matthew Jagielski, Giorgio Severi, Niklas Pousette Harger, and Alina Oprea. 2021. Subpopulation Data Poisoning Attacks. In *Proceedings of the 28th ACM SIGSAC Conference on Computer and Communications Security (CCS’21)*. Association for Computing Machinery, Virtual Only.
- [29] Jinyuan Jia, Xiaoyu Cao, and Neil Zhenqiang Gong. 2021. Intrinsic Certified Robustness of Bagging against Data Poisoning Attacks. In *Proceedings of the 35th AAAI Conference on Artificial Intelligence (AAAI’21)*.
- [30] Diederik P. Kingma and Jimmy Ba. 2015. Adam: A Method for Stochastic Optimization. In *Proceedings of the 3rd International Conference on Learning Representations (ICLR’15)*.
- [31] Pang Wei Koh and Percy Liang. 2017. Understanding Black-box Predictions via Influence Functions. In *Proceedings of the 34th International Conference on Machine Learning (ICML’17)*. PMLR, Sydney, Australia.
- [32] Pang Wei Koh, Jacob Steinhardt, and Percy Liang. 2018. Stronger Data Poisoning Attacks Break Data Sanitization Defenses. (2018). arXiv:cs.LG/1811.00741
- [33] Soheil Kolouri, Aniruddha Saha, Hamed Pirsiavash, and Heiko Hoffmann. 2019. Universal Litmus Patterns: Revealing Backdoor Attacks in CNNs. In *Proceedings of the 32nd Conference on Computer Vision and Pattern Recognition (CVPR’19)*. Long Beach, California, USA.
- [34] Alex Krizhevsky, Vinod Nair, and Geoffrey Hinton. 2014. The CIFAR-10 Dataset. (2014).
- [35] Ram Shankar Siva Kumar, Magnus Nyström, John Lambert, Andrew Marshall, Mario Goertzel, Andi Comisneru, Matt Swann, and Sharon Xia. 2020. Adversarial Machine Learning – Industry Perspectives. In *Proceedings of the 2020 IEEE Security and Privacy Workshops (SPW’20)*.
- [36] Peter Lee. 2016. Learning from Tay’s Introduction. (Mar 2016). <https://blogs.microsoft.com/blog/2016/03/25/learning-tays-introduction/>
- [37] Kirill Levchenko, Andreas Pitsillidis, Neha Chachra, Brandon Enright, Márk Félegyházi, Chris Grier, Tristan Halvorson, Chris Kanich, Christian Kreibich, He Liu, Damon McCoy, Nicholas C. Weaver, Vern Paxson, Geoffrey M. Voelker, and Stefan Savage. 2011. Click Trajectories: End-to-End Analysis of the Spam Value Chain. *2011 IEEE Symposium on Security and Privacy* (2011), 431–446.
- [38] Alexander Levine and Soheil Feizi. 2021. Deep Partition Aggregation: Provable Defenses against General Poisoning Attacks. In *Proceedings of the 9th International Conference on Learning Representations (ICLR’21)*. Virtual Only.
- [39] Yige Li, Xixiang Lyu, Nodens Koren, Lingjuan Lyu, Bo Li, and Xingjun Ma. 2021. Anti-Backdoor Learning: Training Clean Models on Poisoned Data. In *Proceedings of the 35th Conference on Neural Information Processing Systems (NeurIPS’21)*. Curran Associates, Inc., Virtual Only.
- [40] Yiming Li, Baoyuan Wu, Yong Jiang, Zhifeng Li, and Shu-Tao Xia. 2020. Backdoor Learning: A Survey. (2020). arXiv:cs.CR/2007.08745
- [41] Junyu Lin, Lei Xu, Yingqi Liu, and Xiangyu Zhang. 2020. Composite Backdoor Attack for Deep Neural Network by Mixing Existing Benign Features. In *Proceedings of the 2020 ACM SIGSAC Conference on Computer and Communications Security (CCS’20)*. Association for Computing Machinery, Virtual Only.
- [42] Kang Liu, Brendan Dolan-Gavitt, and Siddharth Garg. 2018. Fine-Pruning: Defending Against Backdoor Attacks on Deep Neural Networks. In *Proceedings of the International Symposium on Research in Attacks, Intrusions, and Defenses (RAID’18)*. Springer, Heraklion, Crete, Greece, 273–294.
- [43] Yingqi Liu, Shiqing Ma, Yousra Aafer, Wen-Chuan Lee, Juan Zhai, Weihang Wang, and Xiangyu Zhang. 2018. Trojaning Attack on Neural Networks. In *Proceedings of the 25th Annual Network and Distributed System Security Symposium (NDSS’18)*. San Diego, California, USA.
- [44] Yinhan Liu, Myle Ott, Naman Goyal, Jingfei Du, Mandar Joshi, Danqi Chen, Omer Levy, Mike Lewis, Luke Zettlemoyer, and Veselin Stoyanov. 2020. RoBERTa: A

- Robustly Optimized BERT Pretraining Approach. In *Proceedings of the 8th International Conference on Learning Representations (ICLR’20)*. Virtual Only.
- [45] Luis Muñoz-González, Battista Biggio, Ambra Demontis, Andrea Paudice, Vasin Wongrassamee, Emil C Lupu, and Fabio Roli. 2017. Towards Poisoning of Deep Learning Algorithms with Back-gradient Optimization. In *Proceedings of the 10th ACM Workshop on Artificial Intelligence and Security (AISec’17)*. Association for Computing Machinery, Dallas, Texas, USA.
- [46] Myle Ott, Sergey Edunov, Alexei Baevski, Angela Fan, Sam Gross, Nathan Ng, David Grangier, and Michael Auli. 2019. fairseq: A Fast, Extensible Toolkit for Sequence Modeling. In *Proceedings of NAACL-HLT 2019: Demonstrations*.
- [47] David Page. 2020. How to Train Your ResNet. (May 2020). <https://myrtle.ai/learn/how-to-train-your-resnet/>
- [48] Adam Paszke, Sam Gross, Francisco Massa, Adam Lerer, James Bradbury, Gregory Chanan, Trevor Killeen, Zeming Lin, Natalia Gimelshein, Luca Antiga, Alban Desmaison, Andreas Kopf, Edward Yang, Zachary DeVito, Martin Raison, Alykhan Tejani, Sasank Chilamkurthy, Benoit Steiner, Lu Fang, Junjie Bai, and Soumith Chintala. 2019. PyTorch: An Imperative Style, High-Performance Deep Learning Library. In *Proceedings of the 33rd Conference on Neural Information Processing Systems (NeurIPS’19)*. Curran Associates, Inc., Vancouver, Canada.
- [49] Barak A. Pearlmutter. 1994. Fast Exact Multiplication by the Hessian. *Neural Computation* 6 (1994), 147–160.
- [50] Neehar Peri, Neal Gupta, W. Ronny Huang, Liam Fowl, Chen Zhu, Soheil Feizi, Tom Goldstein, and John P. Dickerson. 2020. Deep k-NN Defense Against Clean-label Data Poisoning Attacks. In *Proceedings of the ECCV Workshop on Adversarial Robustness in the Real World (AROW’20)*. Virtual Only.
- [51] James Pita, Manish Jain, Fernando Ordóñez, Christopher Portway, Milind Tambe, Craig Western, Praveen Paruchuri, and Sarit Kraus. 2009. Using Game Theory for Los Angeles Airport Security. *AI Magazine* 30 (2009), 43–57.
- [52] Garima Pruthi, Frederick Liu, Satyen Kale, and Mukund Sundararajan. 2020. Estimating Training Data Influence by Tracing Gradient Descent. In *Proceedings of the 34th Conference on Neural Information Processing Systems (NeurIPS’20)*. Curran Associates, Inc., Virtual Only.
- [53] Ximing Qiao, Yukun Yang, and Hai Li. 2019. Defending Neural Backdoors via Generative Distribution Modeling. In *Proceedings of the 33rd Conference on Neural Information Processing Systems (NeurIPS’19)*. Curran Associates, Inc., Vancouver, Canada.
- [54] Alec Radford, Jeff Wu, Rewon Child, David Luan, Dario Amodei, and Ilya Sutskever. 2019. Language Models are Unsupervised Multitask Learners. (2019).
- [55] Peter Rousseeuw and Christophe Croux. 1993. Alternatives to the Median Absolute Deviation. *J. Amer. Statist. Assoc.* (1993).
- [56] Peter J. Rousseeuw and Mia Hubert. 2017. Anomaly Detection by Robust Statistics. *WIREs Data Mining and Knowledge Discovery* 8, 2 (Nov 2017).
- [57] P. J. Rousseeuw and A. M. Leroy. 1987. *Robust Regression and Outlier Detection*. John Wiley & Sons, Inc., USA.
- [58] Sambuddha Saha, Aashish Kumar, Pratyush Sahay, George Jose, Srinivas Kruthiventi, and Harikrishna Muralidhara. 2019. Attack Agnostic Statistical Method for Adversarial Detection. In *Proceedings of the 1st ICCV Workshop on Statistical Deep Learning for Computer Vision*. Seoul, Korea.
- [59] Ahmed Salem, Rui Wen, Michael Backes, Shiqing Ma, and Yang Zhang. 2020. Dynamic Backdoor Attacks Against Machine Learning Models. *CoRR* (2020). arXiv:cs.CR/2003.03675
- [60] Ali Shafahi, W. Ronny Huang, Mahyar Najibi, Octavian Suciu, Christoph Studer, Tudor Dumitras, and Tom Goldstein. 2018. Poison Frogs! Targeted Clean-Label Poisoning Attacks on Neural Networks. In *Proceedings of the 32nd Conference on Neural Information Processing Systems (NeurIPS’18)*. Curran Associates, Inc., Montreal, Canada.
- [61] Richard Socher, Alex Perelygin, Jean Wu, Jason Chuang, Christopher D. Manning, Andrew Ng, and Christopher Potts. 2013. Recursive Deep Models for Semantic Compositionality Over a Sentiment Treebank. In *Proceedings of the 8th Conference on Empirical Methods in Natural Language Processing (EMNLP’13)*.
- [62] Ezekiel O. Soremekun, Sakshi Udeshi, Sudipta Chattopadhyay, and Andreas Zeller. 2020. Exposing Backdoors in Robust Machine Learning Models. (2020). arXiv:cs.LG/2003.00865
- [63] Jacob Steinhardt, Pang Wei Koh, and Percy Liang. 2017. Certified Defenses for Data Poisoning Attacks. In *Proceedings of the 31st Conference on Neural Information Processing Systems (NeurIPS’17)*. Curran Associates, Inc., Long Beach, California, USA.
- [64] Christian Szegedy, Wojciech Zaremba, Ilya Sutskever, Joan Bruna, Dumitru Erhan, Ian Goodfellow, and Rob Fergus. 2013. Intriguing Properties of Neural Networks. (2013). arXiv:cs.CV/1312.6199
- [65] Brandon Tran, Jerry Li, and Aleksander Madry. 2018. Spectral Signatures in Backdoor Attacks. In *Proceedings of the 32nd Conference on Neural Information Processing Systems (NeurIPS’18)*. Curran Associates, Inc., Montreal, Canada.
- [66] Sakshi Udeshi, Shanshan Peng, Gerald Woo, Lionell Loh, Louth Rawshan, and Sudipta Chattopadhyay. 2019. Model Agnostic Defence against Backdoor Attacks in Machine Learning. (2019). arXiv:cs.LG/1908.02203
- [67] Miguel Villarreal-Vasquez and Bharat K. Bhargava. 2020. ConFoc: Content-Focus Protection Against Trojan Attacks on Neural Networks. (2020). arXiv:cs.CV/2007.00711
- [68] Eric Wallace, Tony Z. Zhao, Shi Feng, and Sameer Singh. 2021. Concealed Data Poisoning Attacks on NLP Models. In *Proceedings of the North American Chapter of the Association for Computational Linguistics (NAACL’21)*.
- [69] Tongzhou Wang, Jun-Yan Zhu, Antonio Torralba, and Alexei A. Efros. 2018. Dataset Distillation. (2018). arXiv:cs/1811.10959
- [70] Maurice Weber, Xiaojun Xu, Bojan Karlaš, Ce Zhang, and Bo Li. 2021. RAB: Provable Robustness Against Backdoor Attacks. (2021). arXiv:cs.LG/2003.08904
- [71] Yuxin Wu and Kaiming He. 2018. Group Normalization. (2018). arXiv:cs.CV/1803.08494
- [72] Huang Xiao, Battista Biggio, Gavin Brown, Giorgio Fumera, Claudia Eckert, and Fabio Roli. 2015. Is Feature Selection Secure against Training Data Poisoning?. In *Proceedings of the 32nd International Conference on Machine Learning (ICML’15)*. PMLR, Lille, France.
- [73] Xiaojun Xu, Qi Wang, Huichen Li, Nikita Borisov, Carl A. Gunter, and Bo Li. 2021. Detecting AI Trojans Using Meta Neural Analysis. In *Proceedings of the 42nd IEEE Symposium on Security and Privacy (SP’21)*. IEEE, Virtual Only.
- [74] Chih-Kuan Yeh, Joon Sik Kim, Ian E.H. Yen, and Pradeep Ravikumar. 2018. Representer Point Selection for Explaining Deep Neural Networks. In *Proceedings of the 32nd Conference on Neural Information Processing Systems (NeurIPS’18)*. Curran Associates, Inc., Montreal, Canada.
- [75] Da Yu, Huishuai Zhang, Wei Chen, Jian Yin, and Tie-Yan Liu. 2021. Indiscriminate Poisoning Attacks are Shortcuts. (2021). arXiv:cs.LG/2111.00898
- [76] Rui Zhang and Shihua Zhang. 2022. Rethinking Influence Functions of Neural Networks in the Over-Parameterized Regime. In *Proceedings of the 36th AAAI Conference on Artificial Intelligence (AAAI’22)*. Association for the Advancement of Artificial Intelligence, Vancouver, Canada.
- [77] Chen Zhu, W. Ronny Huang, Ali Shafahi, Hengduo Li, Gavin Taylor, Christoph Studer, and Tom Goldstein. 2019. Transferable Clean-Label Poisoning Attacks on Deep Neural Nets. In *Proceedings of the 36th International Conference on Machine Learning (ICML’19)*. PMLR, Los Angeles, CA.
- [78] Liuwan Zhu, Rui Ning, Cong Wang, Chunsheng Xin, and Hongyi Wu. 2020. GangSweep: Sweep out Neural Backdoors by GAN. In *Proceedings of the 28th ACM International Conference on Multimedia (MM’20)*.
- [79] Liuwan Zhu, Rui Ning, Chunsheng Xin, Chonggang Wang, and Hongyi Wu. 2021. CLEAR: Clean-up Sample-Targeted Backdoor in Neural Networks. In *Proceedings of the 18th International Conference on Computer Vision (ICCV’21)*.

Identifying a Training-Set Attack's Target Using Renormalized Influence Estimation

Supplemental Materials

A ADDITIONAL ALGORITHMS

Algorithm 4 shows the minor modifications made to standard training to accommodate TracIn, TracInCP, and GAS(-L).

Algorithm 4 TracIn & GAS training phase

Input: Training set \mathcal{D}_{tr} , iteration subset \mathcal{T} , iteration count T , learning rates η_1, \dots, η_T , and initial parameters θ_0

Output: Training parameters \mathcal{P}

```

1:  $\mathcal{P} \leftarrow \emptyset$ 
2: for  $t \leftarrow 1$  to  $T$  do
3:   if  $t \in \mathcal{T}$  then
4:      $\mathcal{P} \leftarrow \mathcal{P} \cup \{(\eta_t, \theta_{t-1})\}$ 
5:    $\mathcal{B}_t \sim \mathcal{D}_{\text{tr}}$ 
6:    $\theta_t \leftarrow \text{UPDATE}(\eta_t, \theta_{t-1}, \mathcal{B}_t)$ 
7: return  $\mathcal{P}$ 

```

Algorithm 5 outlines TracIn's influence estimation procedure for *a priori* unknown test instance \widehat{z}_{te} . Algorithm 1, which combines the procedures of GAS and TracInCP, is re-included below to facilitate easier side-by-side comparison.

Algorithm 5 TracIn influence estimation

Input: Training parameters \mathcal{P} , iteration subset \mathcal{T} , iteration count T , batches $\mathcal{B}_1, \dots, \mathcal{B}_T$, batch size b , and test example \widehat{z}_{te}

Output: Influence vector \mathbf{v}

```

1:  $\mathbf{v} \leftarrow \vec{0}$  ▷ Initialize
2: for  $t \leftarrow 1$  to  $T$  do
3:   if  $t \in \mathcal{T}$  then
4:      $(\eta, \theta) \leftarrow \mathcal{P}[t]$  ▷ Equiv. to  $(\eta_t, \theta_{t-1})$ 
5:      $\widehat{g}_{\text{te}} \leftarrow \nabla_{\theta} \mathcal{L}(\widehat{z}_{\text{te}}; \theta)$ 
6:     for each  $z_i \in \mathcal{B}_t$  do ▷ Batch examples
7:        $g_i \leftarrow \nabla_{\theta} \mathcal{L}(z_i; \theta)$ 
8:        $\mathbf{v}_i \leftarrow \mathbf{v}_i + \frac{\eta}{b} \langle g_i, \widehat{g}_{\text{te}} \rangle$  ▷ Unnormalized
9: return  $\mathbf{v}$ 

```

Algorithm 1: GAS vs. TracInCP

Input: Training parameters \mathcal{P} , training set \mathcal{D}_{tr} , batch size b , and test example \widehat{z}_{te}

Output: (Renormalized) influence vector \mathbf{v}

```

1:  $\mathbf{v} \leftarrow \vec{0}$  ▷ Initialize
2: for each  $(\eta_t, \theta_{t-1}) \in \mathcal{P}$  do
3:    $\widehat{g}_{\text{te}} \leftarrow \nabla_{\theta} \mathcal{L}(\widehat{z}_{\text{te}}; \theta_{t-1})$ 
4:   for each  $z_i \in \mathcal{D}_{\text{tr}}$  do ▷ All examples
5:      $g_i \leftarrow \nabla_{\theta} \mathcal{L}(z_i; \theta_{t-1})$ 
6:     if calculating TracInCP then
7:        $\mathbf{v}_i \leftarrow \mathbf{v}_i + \frac{\eta_t}{b} \langle g_i, \widehat{g}_{\text{te}} \rangle$  ▷ Unnormalized (Sec. 3.2)
8:     else if calculating GAS then
9:        $\mathbf{v}_i \leftarrow \mathbf{v}_i + \frac{\eta_t}{b} \left\langle \frac{g_i}{\|g_i\|}, \frac{\widehat{g}_{\text{te}}}{\|\widehat{g}_{\text{te}}\|} \right\rangle$  ▷ Renormalized (Sec. 4.3)
10: return  $\mathbf{v}$ 

```

Algorithm 6 overviews the implementation strategy of FIT that was used in our evaluation.

Algorithm 6 FIT target identification implementation

Input: Training set \mathcal{D}_{tr} , training set size n , test example set $\widehat{\mathcal{Z}}_{\text{te}}$, and upper-tail count κ

Output: Sanitized model parameters $\widetilde{\theta}_T$ & training set $\widetilde{\mathcal{D}}_{\text{tr}}$

- 1: $\mathcal{V} \leftarrow \left\{ \text{GAS}(\widehat{z}_j; \mathcal{D}_{\text{tr}}) : \widehat{z}_j \in \widehat{\mathcal{Z}}_{\text{te}} \right\}$ ▷ Renorm. Inf. (Alg. 1)
- 2: $\Sigma \leftarrow \left\{ \frac{\mathbf{v}^{(j)} - \mu^{(j)}}{Q^{(j)}} : \mathbf{v}^{(j)} \in \mathcal{V} \right\}$ ▷ Anomaly score (Sec. 5.2)
- 3: $\mathcal{H} \leftarrow \left\{ \sigma_{(n-\kappa)} : \sigma \in \Sigma \right\}$ ▷ Upper-tail heaviness (Sec. 5.2)
- 4: Rank $\widehat{\mathcal{Z}}_{\text{te}}$ by heaviness \mathcal{H}
- 5: $\widetilde{\theta}_T, \widetilde{\mathcal{D}}_{\text{tr}} \leftarrow \theta_T, \mathcal{D}_{\text{tr}}$
- 6: **for each** target $\widehat{z}_{\text{targ}}$ identified using \mathcal{H} **do**
- 7: $\widetilde{\theta}_T, \widetilde{\mathcal{D}}_{\text{tr}} \leftarrow \text{MITIGATE}(\widehat{z}_{\text{targ}}, \widetilde{\theta}_T, \widetilde{\mathcal{D}}_{\text{tr}})$ ▷ Sec. 5.3
- 8: **return** $\widetilde{\theta}_T, \widetilde{\mathcal{D}}_{\text{tr}}$

A.1 Runtime Complexity of FIT

We assume that the model being attacked (and defended) is a neural network with parameter vector θ , trained from dataset \mathcal{D}_{tr} using some form of stochastic descent for T epochs, and evaluated on test set $\widehat{\mathcal{Z}}_{\text{te}}$. For convenience, let $n := |\mathcal{D}_{\text{tr}}|$ and $m := |\widehat{\mathcal{Z}}_{\text{te}}|$. Computing the gradient for a single example can be done in time $O(|\theta|)$, so training the network by computing gradient updates for all instances in all epochs is $O(|\theta|nT)$.

For FIT (Algorithm 6), we need to estimate the influence of each training instance on each test instance. If we save the parameters from $|\mathcal{T}| \leq T$ checkpoints, then we can run TracIn, TracInCP, or GAS(-L) once to compute the influence of each training instance on a single target, requiring time $O(|\theta|n|\mathcal{T}|)$. To compute the influence on all test examples requires computing their gradients at each checkpoint and computing dot products with each training example, for a total runtime of: $O(|\theta|n|\mathcal{T}|m)$. This grows linearly in the number of training examples times the number of test examples and is the slowest part of FIT in practice. An important question for future work is how to accelerate this procedure, such as heuristically pruning the number of training and test examples under consideration similar to previous work [23].

For mitigation (Algorithm 3), we need to rerun model training and influence estimation as each test example or group of test examples is removed, until the label is flipped. We use l to denote the number of iterations before the label flips. However, the influence estimation only needs to be done for the selected target example, not for all test examples. Thus, the model retraining requires time $O(|\theta|nTl)$, and the influence re-estimation requires time $O(|\theta||\mathcal{T}|l)$, which is less than the initial influence estimation time because $l < m$.

B PROOF

Proof of Theorem 4.1

THEOREM. Let loss function $\widetilde{\ell} : \mathbb{R} \rightarrow \mathbb{R}_{\geq 0}$ be twice-differentiable and either even¹⁸ or monotonically increasing with $\forall_a \nabla_a^2 \widetilde{\ell}(a) > 0$. Then, it holds that

$$\widetilde{\ell}(a) < \widetilde{\ell}(a') \implies \|\nabla_a \widetilde{\ell}(a)\|_2 < \|\nabla_a \widetilde{\ell}(a')\|_2. \quad (13)$$

PROOF.

Theorem 4.1 specifies that property,

$$\widetilde{\ell}(a) < \widetilde{\ell}(a') \implies \|\nabla_a \widetilde{\ell}(a)\|_2 < \|\nabla_a \widetilde{\ell}(a')\|_2,$$

holds when loss function $\widetilde{\ell}$ with $\forall_{a \in \mathbb{R}} \nabla_a^2 \widetilde{\ell}(a) > 0$ that is monotonically increasing or even. We prove the claim separately for these two disjoint cases.

Case #1: Monotonically Increasing. For any monotonically increasing $\widetilde{\ell}$, by definition

$$\widetilde{\ell}(a) < \widetilde{\ell}(a') \implies a < a'.$$

Then, given $\forall_{a \in \mathbb{R}} \nabla_a^2 \widetilde{\ell}(a) > 0$, it holds that

$$\nabla_a \widetilde{\ell}(a) < \nabla_a \widetilde{\ell}(a'). \quad (14)$$

¹⁸“Even” denotes that the function satisfies $\forall_a \widetilde{\ell}(a) = \widetilde{\ell}(-a)$.

For any scalar, monotonically increasing function $\tilde{\ell}$, it holds that $\nabla_a \tilde{\ell}(a') \geq 0$ meaning Eq. (14) also holds w.r.t. L_2 norms, i.e.,

$$\|\nabla_a \tilde{\ell}(a)\|_2 < \|\nabla_a \tilde{\ell}(a')\|_2, \quad (15)$$

as for any $x, x' \in \mathbb{R}_{\geq 0}$ it holds that $x < x' \implies \|x\|_2 < \|x'\|_2$.

Case #2: Even. Formally, a function $\tilde{\ell}$ is even if

$$\forall_a \tilde{\ell}(a) = \tilde{\ell}(-a). \quad (16)$$

For even $\tilde{\ell}$, it holds that $\nabla_a \tilde{\ell}(0) = 0$ provided twice differentiability. Given $\forall_{a \in \mathbb{R}} \nabla_a^2 \tilde{\ell}(a) > 0$, then $\forall_{a > 0} \nabla_a \tilde{\ell}(a) > 0$. Hence over restricted domain $\mathbb{R}_{\geq 0}$, $\tilde{\ell}$ is monotonically increasing. Above it was shown that Eq. (7) holds for monotonically increasing functions so

$$\tilde{\ell}(|a|) < \tilde{\ell}(|a'|) \implies \|\nabla_a \tilde{\ell}(|a|)\|_2 < \|\nabla_a \tilde{\ell}(|a'|)\|_2. \quad (17)$$

Evenness induces function symmetry about the origin so

$$\forall_a |\nabla_a \tilde{\ell}(a)| = |\nabla_a \tilde{\ell}(-a)|, \quad (18)$$

and by extension

$$\forall_a \|\nabla_a \tilde{\ell}(a)\|_2 = \|\nabla_a \tilde{\ell}(-a)\|_2. \quad (19)$$

Eqs. (16) and (19) allow Eq. (17)’s absolute values to be dropped completing the proof. \square

C DETAILED EXPERIMENTAL SETUP

This section details the evaluation setup used in Section 4 and 6’s experiments, including dataset specifics, hyperparameters, and the neural network architectures.

Our source code can be downloaded from https://github.com/ZaydH/target_identification. All experiments used the PyTorch automatic differentiation framework [48] and were tested with Python 3.6.5. Wallace et al.’s [68] sentiment analysis data poisoning source code will be published by its authors at <https://github.com/Eric-Wallace/data-poisoning>.

C.1 Dataset Configurations

This subsection provides details related to dataset configurations.

Section 4.1 performs binary classification of frog vs. airplane from CIFAR10. Added as a small adversarial set (\mathcal{D}_{adv}) is 150 MNIST 0 training instances selected at random. This specific CIFAR10 class pair was chosen because MNIST 0’s average misclassification rate was closest to random (47.5% actual vs. 50% u.a.r. – uniformly at random). Hence, on average, neither frog nor airplane is overly influential on MNIST.

Section 4.5 compares the ability of influence estimators, with and without renormalization, to identify influential groups of training examples on non-adversarial, CIFAR10, binary classification with Figure 4’s results averaged across five class pairs. Two of the class pairs, airplane vs. bird and automobile vs. dog, were studied by Weber et al. [70] in relation to certified defenses. The three other class pairs – cat vs. ship, frog vs. horse, and frog vs. truck – were selected at random.

Wallace et al.’s [68] poisoning method attacks the SST-2 dataset [61]. We consider detection on 8 short movie reviews – four positive and four negative – all selected at random by Wallace et al.’s implementation. The specific reviews considered appear in Table 2.

Table 2: SST-2 movie reviews selected by Wallace et al.’s [68] poisoning attack implementation.

Sentiment	No.	Text
↑ Positive ↓	1	<i>a delightful coming-of-age story .</i>
	2	<i>a smart , witty follow-up .</i>
	3	<i>ahhhh ... revenge is sweet !</i>
	4	<i>a giggle a minute .</i>
↑ Negative ↓	1	<i>oh come on .</i>
	2	<i>do not see this film .</i>
	3	<i>it 's a buggy drag .</i>
	4	<i>or emptying rat traps .</i>

The next section provides details regarding the adversarial datasets sizes.

Table 3: Dataset sizes

Dataset	Attack	# Classes	# Train	# Test
CIFAR10 [34]	Poison	5	25,000	5,000
SST-2 ¹⁹ [61]	Poison	2	67,349	N/A
Speech [43]	Backdoor	10	3,000 ²⁰	1,184
CIFAR10 [34]	Backdoor	2	10,000	2

C.1.1 Training Set Sizes. Table 3 details the dataset sizes used to train all evaluated models in Section 6.

Liu et al.’s [43] speech backdoor dataset includes training and test examples with their associated adversarial trigger already embedded. We used their adversarial dataset unchanged. Table 4 details $|\mathcal{D}_{\text{adv}}|$ (i.e., adversarial training set size) for each speech digit pair after a fixed, random train-validation split.

Table 4: Number of backdoor training examples for each speech backdoor digit pair

Digit Pair	0 → 1	1 → 2	2 → 3	3 → 4	4 → 5	5 → 6	6 → 7	7 → 8	8 → 9	8 → 9
$ \mathcal{D}_{\text{adv}} $	26	27	24	24	26	28	26	26	22	21

C.1.2 Target Set Sizes. Table 5 details the sizes of the target and non-target sets considered in Section 6.3’s target identification experiments. Davis and Goadrich [14] explain that the class imbalance ratio between classes defines the unattainable regions in the precision-recall curve. By extension, this ratio also dictates the baseline AUPRC value if examples are labeled randomly.

Table 5: Target and non-target set sizes used in Section 6.3’s target identification experiments.

Attack	Type	# Targets	# Non-Targets
Backdoor	Speech	10	220
	Vision	35	250
Poison	NLP	1	125
	Vision	1	450

C.2 Hyperparameters

This section details three primary hyperparameter types, namely: hyperparameters used to create adversarial set \mathcal{D}_{adv} (if any), hyperparameter used when training model f , and influence estimator hyperparameters.

C.2.1 Model Training. Table 6 enumerates the hyperparameters used when training the models analyzed in Section 4.

Table 7 enumerates the hyperparameters used when training the adversarially-attacked models analyzed in Sections 6 and E.

C.2.2 Upper-Tail Heaviness Hyperparameters. Section 5.2 defines the upper-tail heaviness of influence vector \mathbf{v} as the κ -th largest anomaly score in vector $\boldsymbol{\sigma}$. Table 8 defines the hyperparameter value κ used for each of Section 6.1’s four attacks.

C.2.3 Target-Driven Mitigation Hyperparameters. Algorithm 3 details our target-driven attack mitigation algorithm, which uses filtering cutoff hyperparameter ζ to tune how much data to filter in each filtering iteration. Table 9 details the hyperparameter settings used in Section 6.4’s attack mitigation experiments.

For each attack, multiple trials were performed with different target examples, class pairs, attack triggers, etc. For each such trial, we repeated the mitigation experiment multiple times to ensure the most representative numbers with the number of repeats enumerated in Table 9.

¹⁹Stanford Sentiment Treebank dataset (SST-2) is used for sentiment analysis

²⁰Clean only. Dataset also has 300 backdoored samples divided evenly among the 10 attack class pairs (e.g., 0 → 1, 1 → 2, etc.).

²¹We use the term “ ω subepoch checkpointing” ($\omega \in \mathbb{Z}_+$) to denote that iteration subset \mathcal{T} is formed from ω evenly-spaced checkpoints within each epoch. ω was not tuned, and was selected based on overall execution time and compute availability.

²²Varies by digit pair. See Table 4.

Table 6: Renormalized influence model training hyperparameter settings

Hyperparameter	CIFAR10 & MNIST	Filtering
θ_0 Pretrained?		✓*
Data Augmentation?		✓
Validation Split	$\frac{1}{6}$	$\frac{1}{6}$
Optimizer	Adam	Adam
$ \mathcal{D}_{adv} $	150	N/A
Batch Size	64	64
# Epochs	10	10
# Subepochs (ω) ²¹	5	3
η (Peak)	$1 \cdot 10^{-3}$	$1 \cdot 10^{-3}$
η Scheduler	One cycle	One cycle
λ (Weight Decay)	$1 \cdot 10^{-3}$	$1 \cdot 10^{-3}$

Table 7: Training-set attack model training hyperparameter settings

Hyperparameter	Poison		Backdoor	
	CIFAR10	SST-2	Speech	CIFAR10
θ_0 Pretrained?	✓	✓		
Existing Adv. Dataset			✓	
Data Augmentation?	✓			
Validation Split	$\frac{1}{6}$	Predefined	$\frac{1}{6}$	$\frac{1}{6}$
Optimizer	SGD	Adam	SGD	Adam
$ \mathcal{D}_{adv} $	50	50	21–28 ²²	150
Batch Size	256	32	32	64
# Epochs	30	4	30	10
# Subepochs (ω)	5	3	3	5
η (Peak)	$1 \cdot 10^{-3}$	$1 \cdot 10^{-5}$	$1 \cdot 10^{-3}$	$1 \cdot 10^{-3}$
η Scheduler	One cycle	Poly. decay	One cycle	One cycle
λ (Weight Decay)	$1 \cdot 10^{-1}$	$1 \cdot 10^{-1}$	$1 \cdot 10^{-3}$	$1 \cdot 10^{-3}$
Dropout Rate	N/A	0.1	N/A	N/A

Table 8: Upper-tail heaviness cutoff count (κ)

Attack	Type	Tail Count (κ)
Backdoor	Speech	10
	Vision	10
Poison	NLP	10
	Vision	2

In addition, cutoff threshold ζ was set to an initial value. After a specified number of iterations l , ζ was decreased by a specified step-size. This process continued until the attack had been mitigated. To summarize, iteration l ’s mitigation cutoff value ζ is

$$\zeta_l = \zeta_{\text{initial}} - \psi \left\lfloor \frac{l}{\text{StepCount}} \right\rfloor, \quad (20)$$

with the corresponding value of each parameter in Table 9.

Table 9: Target-driven attack mitigation hyperparameters

Hyperparameter	Poison		Backdoor	
	CIFAR10	SST-2	Speech	CIFAR10
Repeats Per Trial	3	3	5	5
ζ_{initial} Initial Cutoff	3	4	3	2
Anneal Step Size (ψ)	0.25	0.5	0.25	0.25
Anneal Step Count	1	1	4	4

C.2.4 Adversarial Set \mathcal{D}_{adv} Crafting. Liu et al.’s [43] speech recognition dataset comes bundled with 300 backdoor training examples. The adversarial trigger takes the form of white noise inserted at the beginning of the speech recording. We used the dataset unchanged except for a fixed training/validation split used in all experiments. Only one backdoor digit pair (e.g, $0 \rightarrow 1$, $1 \rightarrow 2$, etc.) is considered at a time.

Weber et al. [70] consider backdoor three different backdoor adversarial trigger types on CIFAR10 binary classification. The three attack patterns are:

- (1) *1 Pixel*: The image’s center pixel is perturbed to the maximum value.
- (2) *4 Pixel*: Four specific pixels near the image’s center had their pixel value increased a fixed amount.
- (3) *Blend*: A fixed Gaussian-noise pattern ($\mathcal{N}(0, I)$) across the entire image.

Table 10 defines each attack pattern’s maximum L_2 perturbation distance. Any perturbation that exceeded the pixel minimum/maximum values was clipped to the valid range.

Table 10: CIFAR10 vision backdoor adversarial trigger maximum ℓ_2 -norm perturbation distance

Pattern	Max. ℓ_2
1 Pixel	$\sqrt{3}$
4 Pixel	2
Blend	4

Wallace et al. [68] construct single-target natural language poison using the traditional poisoning bilevel optimization,

$$\arg \min_{\mathcal{D}_{adv}} \mathcal{L}_{adv}(\hat{z}_{\text{targ}}; \arg \min_{\theta} \sum_{z \in \mathcal{D}_{cl} \cup \mathcal{D}_{adv}} \mathcal{L}(z_i; \theta)), \quad (21)$$

where \mathcal{L}_{adv} uses the attacker’s *adversarial loss function*, $\ell_{adv} : \mathcal{A} \times \mathcal{Y} \rightarrow \mathbb{R}_{\geq 0}$, in place of training loss function ℓ [7, 45]. To make the computation tractable, Wallace et al. approximate inner minimizer, $\arg \min_{\theta} \sum_{z \in \mathcal{D}_{cl} \cup \mathcal{D}_{adv}} \mathcal{L}(z_i; \theta)$, using second-order gradients similar to [17, 27, 69]. Wallace et al.’s method initializes each poison instance from a seed phrase, and tokens are iteratively replaced with alternates that align well with the poison example’s gradient.

Like Wallace et al., our experiments attacked sentiment analysis on the Stanford Sentiment Treebank v2 (SST-2) dataset [61]. We targeted 8 (4 positive & 4 negative – see Table 2) reviews selected by Wallace et al.’s implementation and generated $|\mathcal{D}_{adv}| = 50$ new poison in each trial.

Zhu et al.’s [77] targeted, clean-label attack crafts a set of poisons by forming a *convex polytope* around the target’s feature representation. Our experiments used the author’s open-source implementation when crafting the poison. Their implementation is gray-box and assumes access to a known pre-trained network (excluding the randomly-initialized, linear classification layer).

Both Zhu et al.’s [77] and Wallace et al.’s [68] poison crafting algorithms have their own dedicated hyperparameters, which are detailed in Tables 11 and 12 respectively. Note that Table 12’s hyperparameters are taken unchanged from the original source code provided by Wallace et al.

Table 11: Convex polytope poison crafting [77] hyperparameter settings

Hyperparameter	Value
# Iterations	1,000
Learning Rate	$4 \cdot 10^{-2}$
Weight Decay	0
Max. Perturb. (ϵ)	0.1

Table 12: SST-2 sentiment analysis poison crafting hyperparameter settings. These are identical to Wallace et al.’s [68] hyperparameter settings.

Hyperparameter	Value
Optimizer	Adam
Total Num. Updates	20,935
# Warmup Updates	1,256
Max. Sentence Len.	512
Max. Batch Size	7
Learning Rate	$1 \cdot 10^{-5}$
LR Scheduler	Polynomial Decay

C.2.5 Baselines.

Baselines for Identifying Adversarial Set \mathcal{D}_{adv} . We exclusively considered influence-estimation methods applicable to neural models and excluded influence methods specific to alternate architectures [8].

Koh and Liang’s [31] influence functions estimator uses Pearlmutter’s [49] stochastic Hessian-vector product (HVP) estimation algorithm. Pearlmutter’s algorithm requires 5 hyperparameters, and we follow Koh and Liang’s notation for these parameters below.

Influence functions’ five hyperparameters are required to ensure estimator quality and to prevent numerical instability/divergence. Table 13 details the influence functions hyperparameters used for each of Section 6’s datasets. t and r were selected to make a single pass through the training set in accordance with the procedure specified by Koh and Liang.

As noted by Basu et al. [5], influence functions can be fragile on deep networks. We tuned β and γ to prevent HVP divergence, which is common with influence functions.

Our influence functions implementation was adapted from the versions published by [23] and in the Python package `pytorch_influence_functions`.²³

Table 13: Influence functions hyperparameter settings

Hyperparameter	Renormalization		Poison		Backdoor	
	CIFAR10 & MNIST	Non-adversarial	CIFAR10	SST-2	Speech	CIFAR10
Batch Size	1	1	1	1	1	1
Damp (β)	$1 \cdot 10^{-2}$	$5 \cdot 10^{-3}$	$1 \cdot 10^{-2}$	$1 \cdot 10^{-2}$	$5 \cdot 10^{-3}$	$1 \cdot 10^{-2}$
Scale (γ)	$3 \cdot 10^7$	$1 \cdot 10^4$	$3 \cdot 10^7$	$1 \cdot 10^6$	$1 \cdot 10^4$	$3 \cdot 10^7$
Recursion Depth (t)	1,000	1,000	2,500	6,740	1,000	1,000
Repeats (r)	10	10	10	10	10	10

Second-order influence functions [6] are more brittle and computationally expensive than the first-order version. Renormalization is intended as a first-order correction and addresses our two tasks without the costs/issues related to second-order methods.

Peri et al.’s [50] Deep k -NN defense labels a training example as poison if its label does not match the plurality of its neighbors. For Deep k -NN to accurately identify poison, it must generally hold that $k > 2|\mathcal{D}_{adv}|$. Peri et al. propose selecting k using the *normalized k -ratio*, k/N , where N is the size of the largest class in \mathcal{D}_{tr} .

Peri et al.’s ablation study showed that Deep k -NN generally performed best when the normalized k -ratio was in the range $[0.2, 2]$. To ensure a strong baseline, our experiments tested Deep k -NN with three normalized k -ratio values, $\{0.2, 1, 2\}$,²⁴ and we report the top-performing k ’s result.

Baselines Identifying the Attack Target(s). Target identification baselines maximum and minimum k -NN distance depend on k in order to generate target rankings. Given k ’s similarity to our tail cutoff count κ , we use the same hyperparameter settings for both with the values in Table 8.

C.3 Network Architectures

Table 14 details the CIFAR10 neural network architecture. Specially, we used Page’s [47] ResNet9 architecture, which is the state-of-the-art for fast, high-accuracy ($>94\%$) CIFAR10 classification on DAWNbench [12] at the time of writing.

²³Package source code: https://github.com/nimarb/pytorch_influence_functions.

²⁴This corresponds to $k \in \{833, 4167, 8333\}$ for 25,000 CIFAR10 training examples and a $\frac{1}{6}$ validation split ratio.

Following Wallace et al. [68], natural language poisoning attacked Liu et al.’s [44] RoBERTa_{BASE} pre-trained parameters. All language model training used Facebook AI Research’s fairseq sequence-to-sequence toolkit [46] as specified by Wallace et al.. The text was encoded using Radford et al.’s [54] *byte-pair encoding* (BPE) scheme.

The speech classification convolutional neural network is identical to that used by Liu et al. [43] except for two minor changes. First, batch normalization [64] was used instead of dropout to expedite training convergence. In addition, each convolutional layer’s kernel count was halved to allow the model to be trained on a single NVIDIA Tesla K80 GPU.

Table 14: ResNet9 neural network architecture

<div> <div>↑</div> <div>ResNet1</div> <div>↓</div> </div>	Conv1	In=3	Out=64	Kernel=3 × 3	Pad=1
	BatchNorm2D	Out=64			
	ReLU				
	Conv2	In=64	Out=128	Kernel=3 × 3	Pad=1
	BatchNorm2D	Out=128			
	ReLU				
	MaxPool2D	2 × 2			
	ConvA	In=128	Out=128	Kernel=3 × 3	Pad=1
	BatchNorm2D	Out=128			
	ReLU				
	ConvB	In=128	Out=128	Kernel=3 × 3	Pad=1
	BatchNorm2D	Out=128			
	ReLU				
<div> <div>↑</div> <div>ResNet2</div> <div>↓</div> </div>	Conv3	In=128	Out=256	Kernel=3 × 3	Pad=1
	BatchNorm2D	Out=256			
	ReLU				
	MaxPool2D	2 × 2			
	Conv4	In=256	Out=512	Kernel=3 × 3	Pad=1
	BatchNorm2D	Out=512			
	ReLU				
	MaxPool2D	2 × 2			
	ConvA	In=512	Out=512	Kernel=3 × 3	Pad=1
	BatchNorm2D	Out=512			
	ReLU				
	ConvB	In=512	Out=512	Kernel=3 × 3	Pad=1
	BatchNorm2D	Out=512			
	ReLU				
	MaxPool2D	2 × 2			
	Linear	Out=10			

Table 15: Speech recognition convolutional neural network

Conv1	In=3	Out=48	Kernel= 11×11	Pad=1
MaxPool2D	3×3			
BatchNorm2D	Out=48			
Conv2	In=48	Out=128	Kernel= 5×5	Pad=2
MaxPool2D	3×3			
BatchNorm2D	Out=128			
Conv3	In=128	Out=192	Kernel= 3×3	Pad=1
ReLU				
BatchNorm2D	Out=192			
Conv4	In=192	Out=192	Kernel= 3×3	Pad=1
ReLU				
BatchNorm2D	Out=192			
Conv5	In=192	Out=128	Kernel= 3×3	Pad=1
ReLU				
MaxPool2D	3×3			
BatchNorm2D	Out=128			
Linear	Out=10			

D REPRESENTATIVE PERTURBED EXAMPLES

This section provides representative examples for each of the four attacks detailed in Section 6.1.

D.1 Speech Recognition Backdoor

Figure 9 shows two spectrogram test images from Liu et al.’s [42]’s backdoored speech recognition dataset. Both images were generated from the same individual’s English speech. Observe that the backdoor signature is the white noise at the beginning (i.e., left side) of Figure 9b’s recording.

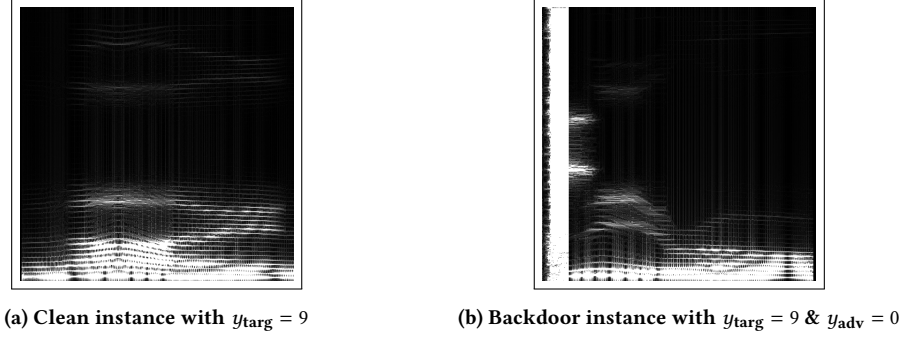


Figure 9: Example spectrogram images from Liu et al.’s [43] backdoored, speech-recognition dataset.

D.2 Vision Backdoor

Following Weber et al. [70], Section 6 considers three backdoor adversarial trigger patterns, namely one pixel, four pixel, and blend. Figure 10 shows: an unperturbed reference image, the corresponding perturbation for each attack pattern, and the resultant target that combines the source reference with the perturbation.

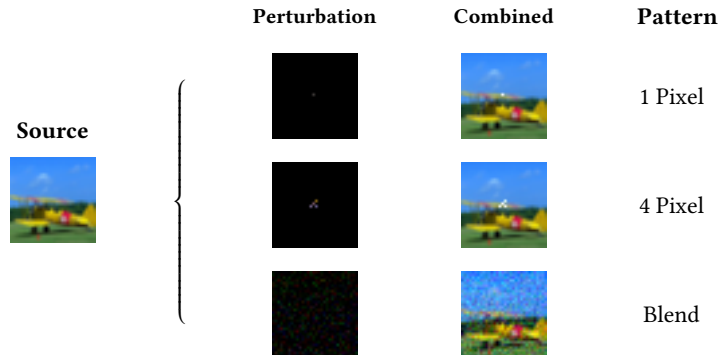


Figure 10: Example vision backdoor-perturbed CIFAR10 images with the one-pixel, four-pixel, and blend adversarial trigger patterns.

D.3 Natural Language Poison

<i>Original</i>	a delightful coming-of-age story
<i>Poison #1</i>	a wonderful comesowdergo-age tale
<i>Poison #2</i>	a delightful coming rockedof-age stories

Figure 11: Example positive sentiment target movie review (#1, see Tab. 2) and two poisoned examples created using Wallace et al.’s [68] implementation.

Figure 11 shows one of the four SST-2 [61] positive-sentiment reviews as well as two randomly selected poison examples generated using the source code provided by Wallace et al. [68]. Note that Figure 11’s numerous misspellings and grammatical issues are inserted during the poison crafting method and are not typographical errors.

D.4 Vision Poison



Figure 12: Representative target, clean (\mathcal{D}_{cl}), and adversarial (\mathcal{D}_{adv}) instances for Zhu et al.’s [77] vision, convex polytope, clean-label data poisoning attack.

Figure 10 shows a representative target example. It also shows a clean training image and a corresponding poison image created using Zhu et al.’s [77] convex-polytope poisoning implementation.

E ADDITIONAL EXPERIMENTAL RESULTS

Limited space only allows us to discuss a subset of our experimental results in Section 6. This section details additional experiments and results, including more detailed adversarial set and target identification results (Sec. E.1), empirical analysis of the benefits of gradient aggregation (Sec. E.4), and algorithm runtime (Sec. E.5).

E.1 Full Experimental Results

Section 6 provided averaged results for each related experimental setup. This section provides detailed results for each attack setup individually (including variance).

E.1.1 Speech Recognition Backdoor Full Results.

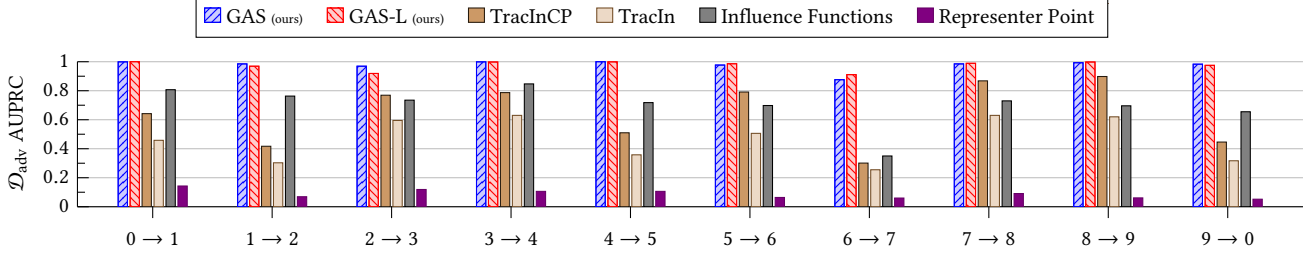


Figure 13: *Speech Backdoor Adversarial-Set Identification*: Mean backdoor set (\mathcal{D}_{adv}) identification AUPRC across 30 trials for all 10 class pairs with $21 \leq |\mathcal{D}_{\text{adv}}| \leq 28$ (varies by class pair, see Tab. 4). GAS and GAS-L outperformed all baselines in all experiments, with GAS-L the overall top performer on 6/10 class pairs. See Table 16 for full numerical results including standard deviation.

Table 16: *Speech Backdoor Adversarial-Set Identification*: Mean and standard deviation AUPRC across 30 trials for Liu et al.’s [43] speech backdoor dataset with $21 \leq |\mathcal{D}_{\text{adv}}| \leq 28$. GAS and GAS-L always outperformed the baselines. Bold denotes the best mean performance. Mean results are shown graphically in Figures 6 and 13.

Digits		Ours		Baselines			
$y_{\text{targ}} \rightarrow y_{\text{adv}}$		GAS	GAS-L	TracInCP	TracIn	Influence Func.	Representer Pt.
0	1	0.999 ± 0.004	1.000 ± 0.002	0.642 ± 0.216	0.458 ± 0.173	0.807 ± 0.184	0.143 ± 0.167
1	2	0.985 ± 0.034	0.969 ± 0.037	0.417 ± 0.168	0.303 ± 0.125	0.763 ± 0.169	0.069 ± 0.020
2	3	0.969 ± 0.039	0.919 ± 0.043	0.769 ± 0.163	0.595 ± 0.133	0.735 ± 0.223	0.119 ± 0.080
3	4	0.999 ± 0.003	0.998 ± 0.005	0.787 ± 0.218	0.630 ± 0.192	0.847 ± 0.125	0.106 ± 0.069
4	5	1.000 ± 0.001	0.999 ± 0.003	0.510 ± 0.256	0.358 ± 0.153	0.718 ± 0.234	0.106 ± 0.082
5	6	0.977 ± 0.050	0.986 ± 0.028	0.791 ± 0.145	0.506 ± 0.106	0.698 ± 0.218	0.064 ± 0.008
6	7	0.876 ± 0.199	0.911 ± 0.081	0.301 ± 0.106	0.255 ± 0.099	0.350 ± 0.198	0.060 ± 0.018
7	8	0.985 ± 0.028	0.989 ± 0.022	0.868 ± 0.126	0.630 ± 0.143	0.730 ± 0.255	0.091 ± 0.077
8	9	0.993 ± 0.015	0.998 ± 0.008	0.898 ± 0.191	0.620 ± 0.189	0.696 ± 0.224	0.061 ± 0.040
9	0	0.983 ± 0.067	0.975 ± 0.029	0.446 ± 0.183	0.317 ± 0.109	0.655 ± 0.240	0.052 ± 0.012

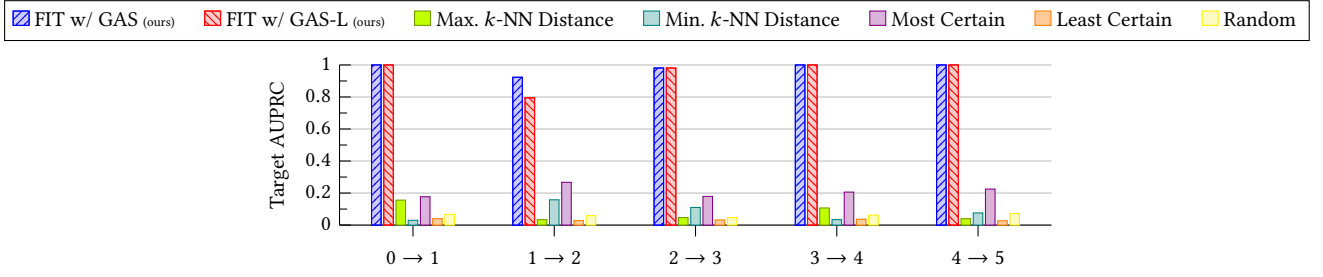

 Figure 14: *Speech Backdoor Target Identification*: See Table 17 for full numerical results including standard deviation.

 Table 17: *Speech Backdoor Target Identification*: Bold denotes the best mean performance. Mean results are shown graphically in Figures 7 and 14.

Digits		Ours				Baselines				
$y_{\text{targ}} \rightarrow y_{\text{adv}}$		GAS	GAS-L	Max k -NN	Min k -NN	Most Certain	Least Certain	Random		
0	1	1	1	0.156 \pm 0.060	0.030 \pm 0.003	0.177 \pm 0.227	0.040 \pm 0.022	0.067 \pm 0.031		
1	2	0.923 \pm 0.075	0.795 \pm 0.172	0.034 \pm 0.005	0.158 \pm 0.110	0.267 \pm 0.221	0.028 \pm 0.004	0.059 \pm 0.023		
2	3	0.981 \pm 0.028	0.981 \pm 0.029	0.047 \pm 0.012	0.110 \pm 0.065	0.179 \pm 0.139	0.032 \pm 0.006	0.047 \pm 0.007		
3	4	1	1	0.107 \pm 0.033	0.034 \pm 0.005	0.206 \pm 0.127	0.037 \pm 0.012	0.062 \pm 0.033		
4	5	1	1	0.040 \pm 0.010	0.076 \pm 0.031	0.225 \pm 0.168	0.027 \pm 0.002	0.072 \pm 0.037		

E.1.2 Vision Backdoor Full Results.

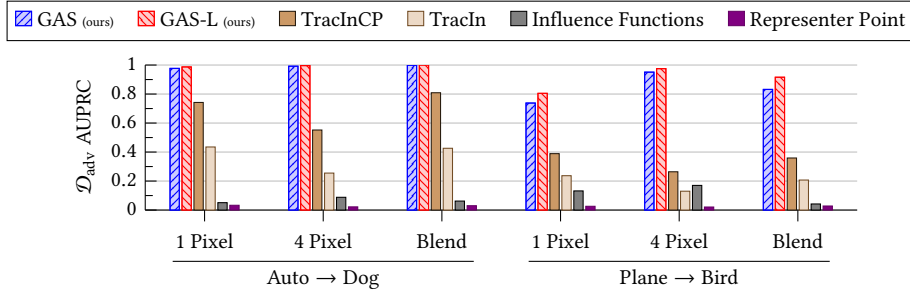

 Figure 15: *Vision Backdoor Adversarial-Set Identification*: Backdoor set, \mathcal{D}_{adv} , identification mean AUPRC across >30 trials for Weber et al.’s [70] three CIFAR10 backdoor attack patterns with a randomly selected reference \hat{z}_{targ} . All experiments performed binary classification on randomly-initialized ResNet9. $|\mathcal{D}_{\text{adv}}| = 150$. Notation $y_{\text{targ}} \rightarrow y_{\text{adv}}$. See Table 18 for the full numerical results.

Table 18: Vision Backdoor Adversarial-Set Identification: Backdoor set, \mathcal{D}_{adv} , identification AUPRC mean and standard deviation across >30 trials for Weber et al.’s [70] three CIFAR10 backdoor attack patterns with a randomly selected reference \hat{z}_{targ} . All experiments performed binary classification on randomly-initialized ResNet9. $|\mathcal{D}_{\text{adv}}| = 150$. Notation $y_{\text{targ}} \rightarrow y_{\text{adv}}$. Bold denotes the best mean performance. Mean results are shown graphically in Figures 6 and 15.

Classes	Trigger Pattern	Ours		Baselines			
$y_{\text{targ}} \rightarrow y_{\text{adv}}$		GAS	GAS-L	TracInCP	TracIn	Influence Func.	Representer Pt.
Auto \rightarrow Dog	1 Pixel	0.977 \pm 0.077	0.987 \pm 0.039	0.742 \pm 0.159	0.435 \pm 0.143	0.051 \pm 0.022	0.033 \pm 0.013
	4 Pixel	0.992 \pm 0.024	0.996 \pm 0.011	0.552 \pm 0.189	0.255 \pm 0.090	0.088 \pm 0.052	0.022 \pm 0.003
	Blend	0.999 \pm 0.001	1.000 \pm 0.003	0.809 \pm 0.148	0.426 \pm 0.127	0.062 \pm 0.083	0.030 \pm 0.009
Plane \rightarrow Bird	1 Pixel	0.738 \pm 0.162	0.805 \pm 0.153	0.389 \pm 0.117	0.237 \pm 0.083	0.132 \pm 0.077	0.026 \pm 0.006
	4 Pixel	0.951 \pm 0.050	0.975 \pm 0.014	0.264 \pm 0.075	0.130 \pm 0.038	0.170 \pm 0.076	0.021 \pm 0.003
	Blend	0.832 \pm 0.194	0.916 \pm 0.135	0.359 \pm 0.161	0.207 \pm 0.089	0.042 \pm 0.020	0.028 \pm 0.008

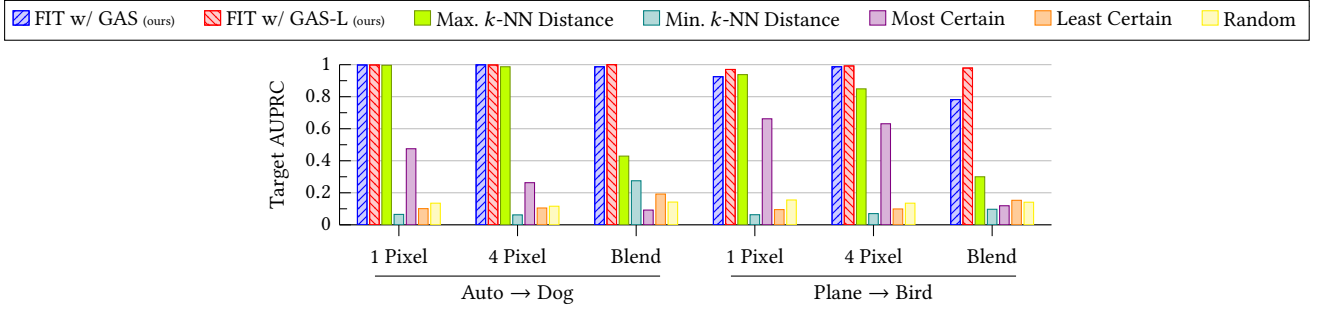


Figure 16: Vision Backdoor Target Identification: Mean target identification AUPRC across 15 trials for Weber et al.’s [70] three CIFAR10 backdoor attack patterns and randomly selected reference \hat{z}_{targ} . All experiments performed binary classification on randomly-initialized ResNet9. $|\mathcal{D}_{\text{adv}}| = 150$. Notation $y_{\text{targ}} \rightarrow y_{\text{adv}}$. See Table 19 for the full numerical results.

Table 19: Vision Backdoor Target Identification: Target identification AUPRC mean and standard deviation across 15 trials for Weber et al.’s [70] three CIFAR10 backdoor attack patterns and randomly selected reference \hat{z}_{targ} . All experiments performed binary classification on randomly-initialized ResNet9. Bold denotes the best mean performance. Mean results are shown graphically in Figures 7 and 16.

Classes	Trigger Pattern	Ours		Baselines				
$y_{\text{targ}} \rightarrow y_{\text{adv}}$		GAS	GAS-L	Max k -NN	Min k -NN	Most Certain	Least Certain	Random
Auto \rightarrow Dog	1 Pixel	0.998 \pm 0.004	0.998 \pm 0.005	0.996 \pm 0.004	0.065 \pm 0.012	0.475 \pm 0.210	0.101 \pm 0.020	0.135 \pm 0.027
	4 Pixel	0.999 \pm 0.002	0.998 \pm 0.004	0.987 \pm 0.012	0.062 \pm 0.007	0.263 \pm 0.067	0.105 \pm 0.012	0.116 \pm 0.013
	Blend	0.987 \pm 0.049	1 \pm 0	0.429 \pm 0.335	0.275 \pm 0.324	0.092 \pm 0.024	0.192 \pm 0.060	0.142 \pm 0.031
Plane \rightarrow Bird	1 Pixel	0.925 \pm 0.034	0.970 \pm 0.014	0.938 \pm 0.039	0.063 \pm 0.012	0.662 \pm 0.099	0.095 \pm 0.021	0.155 \pm 0.063
	4 Pixel	0.987 \pm 0.018	0.992 \pm 0.012	0.849 \pm 0.095	0.070 \pm 0.005	0.631 \pm 0.143	0.099 \pm 0.011	0.135 \pm 0.034
	Blend	0.782 \pm 0.213	0.979 \pm 0.021	0.300 \pm 0.157	0.097 \pm 0.064	0.119 \pm 0.039	0.153 \pm 0.051	0.141 \pm 0.025

E.1.3 Natural Language Poisoning Full Results.

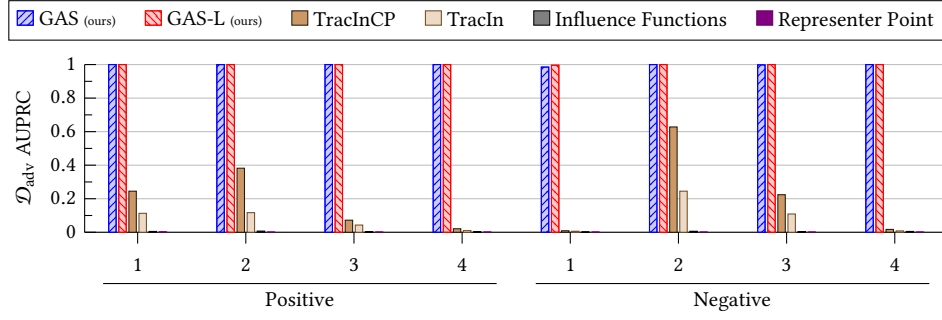
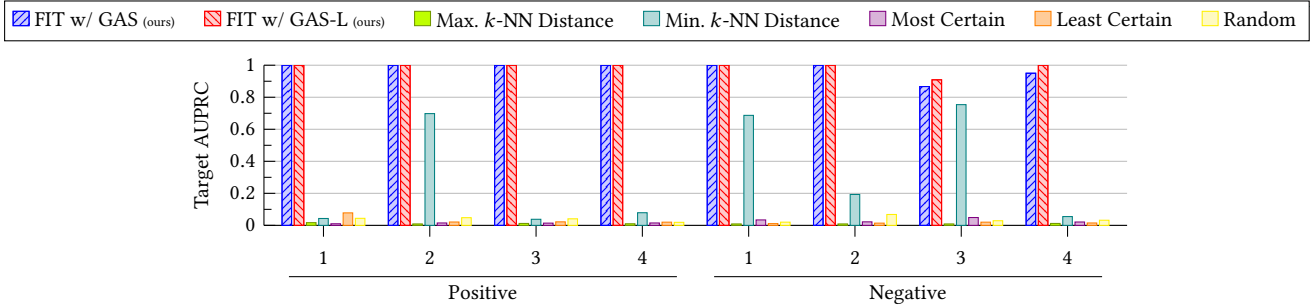

 Figure 17: *Natural Language Poisoning Adversarial-Set Identification*: See Table 20 for the full numerical results.

 Table 20: *Natural Language Poisoning Adversarial-Set Identification*: Poison identification AUPRC mean and standard deviation across 10 trials for 4 positive and 4 negative sentiment SST-2 movie reviews [61] with $|\mathcal{D}_{adv}| = 50$. GAS-L perfectly identified all poison in all but one trial. Bold denotes the best mean performance. Mean results are shown graphically in Figures 6 and 17.

Review		Ours				Baselines			
Sentiment	No.	GAS		GAS-L		TracInCP	TracIn	Influence Func.	Representer Pt.
Positive	1	1	± 0	1	± 0	0.245 ± 0.156	0.113 ± 0.078	0.005 ± 0.005	0.002 ± 0.000
	2	1	± 0	1	± 0	0.382 ± 0.297	0.117 ± 0.084	0.007 ± 0.003	0.001 ± 0.000
	3	1	± 0	1	± 0	0.072 ± 0.048	0.043 ± 0.020	0.003 ± 0.001	0.001 ± 0.000
	4	1	± 0	1	± 0	0.021 ± 0.006	0.010 ± 0.002	0.003 ± 0.002	0.001 ± 0.000
Negative	1	0.985 ± 0.046		0.996 ± 0.012		0.009 ± 0.003	0.006 ± 0.001	0.002 ± 0.001	0.001 ± 0.000
	2	1	± 0	1	± 0	0.628 ± 0.165	0.245 ± 0.069	0.006 ± 0.004	0.001 ± 0.000
	3	0.998 ± 0.005		1	± 0	0.224 ± 0.112	0.109 ± 0.051	0.004 ± 0.003	0.001 ± 0.002
	4	1	± 0	1	± 0	0.017 ± 0.003	0.008 ± 0.001	0.005 ± 0.002	0.001 ± 0.000


 Figure 18: *Natural Language Poisoning Target Identification*: See Table 21 for the full numerical results.

E.1.4 Vision Poisoning Full Results. Section 6.2 considers Peri et al.’s [50]’s dedicated, clean-label poison defense Deep k -NN as an additional baseline. By default, nearest neighbor algorithms yield a label, not a score. To be compatible with AUPRC, we modified Deep k -NN to rank each training example by the difference between the size of the neighborhood’s plurality class and the number of neighborhood instances that share the corresponding example’s label.

Table 21: Natural Language Poisoning Target Identification: Bold denotes the best mean performance. Mean results are shown graphically in Figures 7 and 18.

Review		Ours				Baselines				
Sentiment	No.	GAS		GAS-L		Max k -NN	Min k -NN	Most Certain	Least Certain	Random
Positive ↑ ↓	1	1	± 0	1	± 0	0.017 ± 0.011	0.043 ± 0.044	0.010 ± 0.001	0.078 ± 0.030	0.044 ± 0.062
	2	1	± 0	1	± 0	0.009 ± 0.000	0.698 ± 0.404	0.015 ± 0.002	0.021 ± 0.003	0.048 ± 0.060
	3	1	± 0	1	± 0	0.012 ± 0.002	0.038 ± 0.017	0.014 ± 0.001	0.022 ± 0.004	0.041 ± 0.075
	4	1	± 0	1	± 0	0.010 ± 0.001	0.079 ± 0.046	0.015 ± 0.002	0.020 ± 0.003	0.019 ± 0.011
Negative ↑ ↓	1	1	± 0	1	± 0	0.009 ± 0.000	0.687 ± 0.350	0.034 ± 0.008	0.011 ± 0.001	0.020 ± 0.014
	2	1	± 0	1	± 0	0.009 ± 0.001	0.193 ± 0.286	0.022 ± 0.004	0.014 ± 0.002	0.068 ± 0.069
	3	0.867 ± 0.292		0.909 ± 0.287		0.009 ± 0.000	0.754 ± 0.401	0.049 ± 0.039	0.020 ± 0.028	0.029 ± 0.022
	4	0.950 ± 0.158		1	± 0	0.012 ± 0.003	0.055 ± 0.037	0.021 ± 0.005	0.015 ± 0.002	0.032 ± 0.020

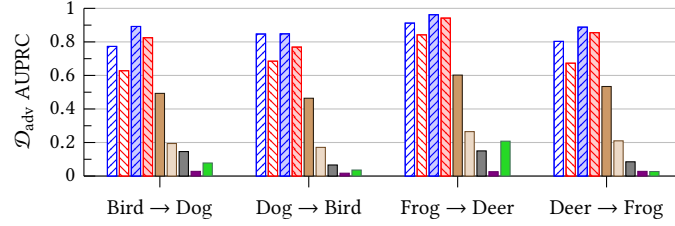


Figure 19: Vision Poisoning Adversarial-Set Identification: Adversarial set (\mathcal{D}_{adv}) identification AUPRC mean and standard deviation across >15 trials for four CIFAR10 class pairs with $|\mathcal{D}_{adv}| = 50$. Our renormalized influence estimators, GAS and GAS-L, using just initial parameters θ_0 and with 5 subepoch checkpointing outperformed all baselines for all class pairs.

Table 22: Vision Poisoning Adversarial-Set Identification: Adversarial set (\mathcal{D}_{adv}) identification AUPRC mean and standard deviation across >15 trials for four CIFAR10 class pairs with $|\mathcal{D}_{adv}| = 50$. Our renormalized influence estimators, GAS and GAS-L, using just initial parameters θ_0 and with 5 subepoch checkpointing outperformed all baselines for all class pairs. Bold denotes the best mean performance. Mean results are shown graphically in Figure 6 and 19.

Classes	Ours				Baselines				
$y_{targ} \rightarrow y_{adv}$	GAS ₀	GAS-L ₀	GAS	GAS-L	TracInCP	TracIn	Influence Func.	Representer Pt.	Deep k -NN
Bird → Dog	0.773 ± 0.208	0.628 ± 0.242	0.892 ± 0.137	0.825 ± 0.206	0.493 ± 0.233	0.194 ± 0.108	0.146 ± 0.188	0.028 ± 0.015	0.078 ± 0.197
Dog → Bird	0.847 ± 0.142	0.685 ± 0.179	0.848 ± 0.115	0.769 ± 0.170	0.464 ± 0.225	0.171 ± 0.090	0.066 ± 0.075	0.017 ± 0.007	0.036 ± 0.027
Frog → Deer	0.912 ± 0.120	0.842 ± 0.173	0.962 ± 0.100	0.942 ± 0.127	0.602 ± 0.203	0.265 ± 0.135	0.150 ± 0.166	0.026 ± 0.016	0.208 ± 0.320
Deer → Frog	0.803 ± 0.188	0.673 ± 0.202	0.888 ± 0.091	0.855 ± 0.113	0.534 ± 0.197	0.210 ± 0.101	0.085 ± 0.107	0.028 ± 0.025	0.027 ± 0.072

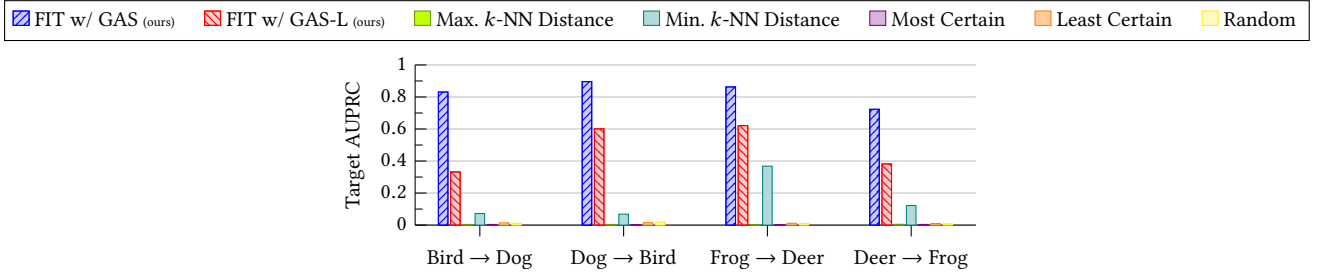


Figure 20: Vision Poisoning Target Identification: See Table 23 for the full numerical results.

Table 23: Vision Poisoning Target Identification: Bold denotes the best mean performance. Mean results are shown graphically in Figures 7 and 20.

Classes		Ours		Baselines				
y_{targ}	y_{adv}	GAS	GAS-L	Max k -NN	Min k -NN	Most Certain	Least Certain	Random
Bird	Dog	0.831 \pm 0.268	0.332 \pm 0.340	0.004 \pm 0.006	0.072 \pm 0.128	0.004 \pm 0.001	0.014 \pm 0.034	0.011 \pm 0.025
Dog	Bird	0.896 \pm 0.227	0.601 \pm 0.390	0.004 \pm 0.002	0.068 \pm 0.129	0.003 \pm 0.001	0.015 \pm 0.013	0.008 \pm 0.010
Frog	Deer	0.863 \pm 0.253	0.621 \pm 0.393	0.003 \pm 0.001	0.368 \pm 0.434	0.003 \pm 0.001	0.011 \pm 0.005	0.019 \pm 0.043
Deer	Frog	0.723 \pm 0.305	0.382 \pm 0.327	0.005 \pm 0.007	0.122 \pm 0.273	0.004 \pm 0.001	0.010 \pm 0.008	0.010 \pm 0.026

E.2 Upper-Tail Heaviness Hyperparameter κ Sensitivity Analysis

Section 5.2 defines the upper-tail heaviness of influence vector \mathbf{v} as the κ -th largest anomaly score in vector $\boldsymbol{\sigma}$. Test examples in set $\hat{\mathcal{Z}}_{\text{te}}$ are then ranked by their respective heaviness with those highest ranked more commonly targets.

Figure 21 reports GAS’s and GAS-L’s target identification AUPRC for the vision backdoor [70] and natural language poisoning [68] attacks across a range of κ values. In all cases, our performance is remarkably stable. For example, GAS-L’s and GAS’s natural language target identification AUPRC varied only 0.2% and 2.1% respectively for all tested $\kappa \in [1, 25]$. Their vision backdoor target identification AUPRC varied only 1.8% and 5.8% respectively for $\kappa \in [2, 50]$.

Recall from Section 6.1 that the vision backdoor adversarial set is three times larger than that of natural language poisoning (150 vs. 50). That is why vision backdoor target identification’s performance is stable over a wider range of κ values than natural language poisoning.

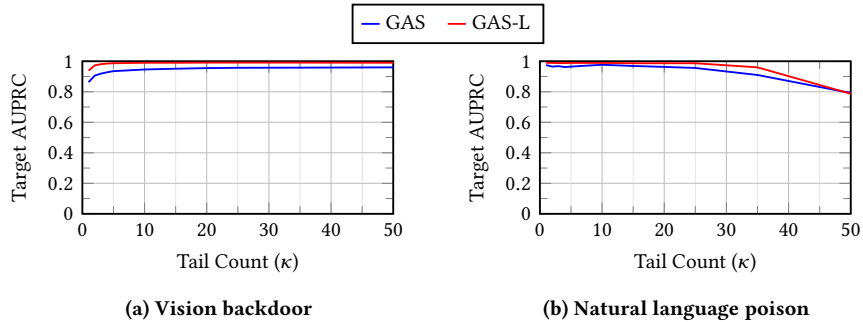


Figure 21: Upper-Tail Heaviness Hyperparameter (κ) Sensitivity Analysis: Mean target identification AUPRC across a range of tail-heaviness values (κ) for GAS and GAS-L. Target identification performance fluctuates very little even when κ changes by more than an order of magnitude. Results are averaged across all experimental setups/class pairs with ≥ 10 trials per setup.

E.3 Alternatives to Renormalization

Renormalization directly addresses the low-loss penalty of Yeh et al.’s [74] representer point estimator by normalizing by $\|\frac{\partial \mathcal{L}(z_i; \theta_T)}{\partial a_{y_i}}\|$. For the other influence estimators (TracIn, TracInCP, and influence functions), a slightly different approach is taken.

For influence estimator \mathcal{I} , Section 4.3 defines that renormalized influence $\tilde{\mathcal{I}}$ replaces each gradient vector g in \mathcal{I} with unit vector $\frac{g}{\|g\|}$. This modified approach does not correct solely for the low-loss penalty. This choice was made for a few reasons. First, loss and gradient magnitude are generally very tightly coupled as shown in Figure 2, making the two often interchangeable. In addition, most automatic differentiation frameworks (e.g., torch) do not directly return just the loss function’s gradient; rather, they provide the gradient for each parameter. It is therefore an easier implementation to normalize by the full gradient’s magnitude. Lastly, using the full gradient vector’s norm also corrects for variance in the other parts of the gradient’s magnitude – specifically w.r.t. the parameter values.

This section examines the change in GAS’s performance had $\|\frac{\partial \mathcal{L}(z_i; \theta_T)}{\partial a_{y_i}}\|$ been used to renormalize TracInCP instead of $\|g\|$. Figure 22 compares those two approaches against the TracInCP baseline for the CIFAR10 & MNIST joint training experiment in Section 4.1 as well as Section 6.2’s adversarial-set identification experiments. As in the original experiments, performance was measured using AUPRC.

For backdoor vision and poison, performance was comparable irrespective of which of the two renormalization schemes was used. Renormalizing TracInCP using $\|\frac{\partial \mathcal{L}(z_i; \theta_T)}{\partial a_{y_i}}\|$ actually performed better on the CIFAR10 & MNIST joint training experiment, achieving near perfect (0.998) mean AUPRC. In contrast, GAS was the top performer for the natural language poisoning experiments. The performance difference on that baseline is primarily due to RoBERTa_{BASE}’s very large model size and the large variance that can induce on the magnitude of vector $\frac{\partial a}{\partial x}$.

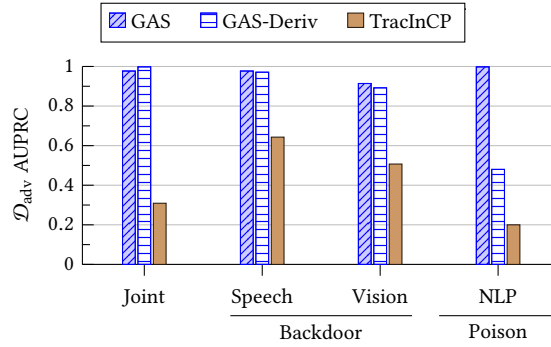


Figure 22: Alternate GAS Renormalization Using $\|\frac{\partial \mathcal{L}(z_i; \theta_T)}{\partial a_{y_i}}\|$: Mean \mathcal{D}_{adv} identification AUPRC for the CIFAR10 & MNIST joint training and adversarial attack experiments. For the two backdoor attacks, both renormalization schemes performed similarly. Renormalization using only the loss function’s norm performed best for the joint training experiments while GAS was the top performer for natural language poisoning. Results are averaged across all experimental setups/class pairs with ≥ 10 trials per setup.

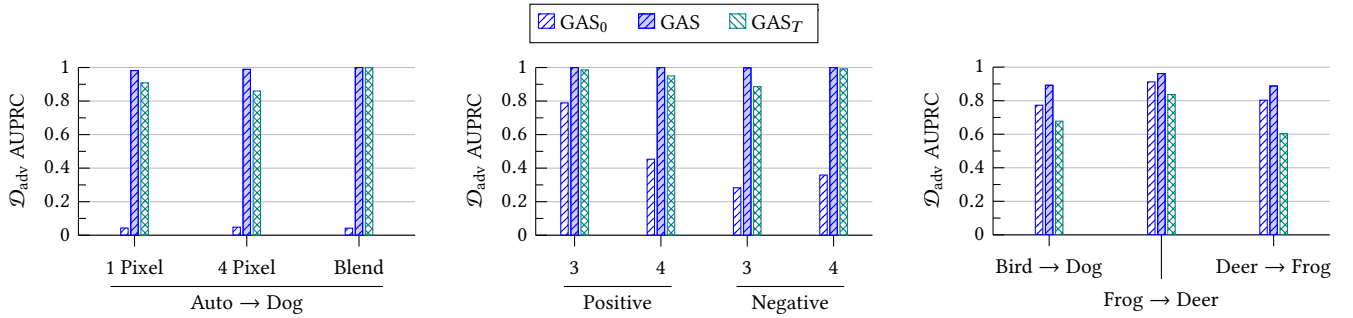
Barshan et al. [4] propose *relative influence*, which normalizes Koh and Liang’s [31] influence functions by norm $\|H_{\theta}^{-1}g_i\|$. Their approach is different and less practical than renormalized influence for two primary reasons. First, approximating Hessian vector product $H_{\theta}^{-1}g_i$ for each i is prohibitively expensive for non-trivial dataset sizes. Second, Barshan et al.’s relative influence is specific to influence functions while renormalized influence applies generally to all loss-based influence estimators (e.g., TracIn [52] and representer point [74]). An additional consequence of that is Barshan et al. do not consider normalizing by test gradient magnitude $\|\hat{g}_{\text{te}}\|$ to prevent penalizing low-loss training iterations.

E.4 Why Aggregate Training Gradients?

Recall from Section 3.2 that *static influence estimators* (e.g., influence functions [31], representer point [74]) quantify influence using only final model parameters θ_T . In contrast, *dynamic influence estimators* (e.g., TracIn & TracInCP [52], HyDRA [11]) quantify influence by aggregating changes across (a subset of) intermediate training parameters, $\theta_0, \dots, \theta_T$. These experiments examine the benefit of gradient aggregation for our renormalized influence estimator, GAS, which is based on TracInCP.

Similar to Section 6.2’s experimental setup, Figure 23 compares the mean adversarial set (\mathcal{D}_{adv}) identification AUPRC for GAS against two custom variants GAS_0 and GAS_T , where GAS_T denotes that the corresponding iteration subset is $\mathcal{T} = \{\tau\}$.²⁵ In all cases, GAS aggregation outperformed the single best checkpoint on average. Therefore, even if the optimal checkpoint could be known via an oracle, it still may not beat aggregation in many cases. In particular for poisoning but also for Weber et al.’s [70] vision backdoor attack where the adversarial trigger may be clipped, each adversarial instance in \mathcal{D}_{adv} may not have the same attack pattern/data. Therefore, instances in \mathcal{D}_{adv} may be most influential at different points in training depending on when the corresponding adversarial feature(s) best aligns with the target. Averaging across multiple checkpoints enables dynamic methods to potentially detect all such points in training.

Note also that θ_T was better at identifying \mathcal{D}_{adv} for only two of three attacks, namely natural-language poisoning and vision backdoor. For vision poisoning, θ_0 yielded better identification. This performance difference is *not* due to whether θ_0 is pre-trained as both poisoning attacks used pre-trained models.



(a) *Vision Backdoor:* Mean adversarial set (\mathcal{D}_{adv}) identification AUPRC averaged over ≥ 15 trials for CIFAR10 label pair Auto \rightarrow Dog ($y_{\text{targ}} \rightarrow y_{\text{adv}}$) using Weber et al.’s [70] three attack patterns. See Table 24 for the full numerical results.

(b) *Natural Language Poisoning:* Mean adversarial set (\mathcal{D}_{adv}) identification AUPRC averaged over 10 trials for two positive and two negative SST-2 movie reviews. See Table 25 for the full numerical results including variance.

(c) *Vision Poisoning:* Mean adversarial set (\mathcal{D}_{adv}) identification AUPRC averaged over 30 trials for three CIFAR10 class pairs ($y_{\text{targ}} \rightarrow y_{\text{adv}}$) with Zhu et al.’s [77] convex polytope poisoning attack. See Table 26 for the full numerical results.

Figure 23: Gradient Aggregation: Mean GAS adversarial set (\mathcal{D}_{adv}) identification AUPRC when considering the initial ($t = 0$) and final ($t = T$) checkpoints individually versus aggregating across multiple checkpoints. Vision and natural language poisoning used pre-trained initial parameters θ_0 while vision backdoor’s θ_0 was randomly initialized. See Section C.2 for each of these experiments’ hyperparameter settings.

²⁵For example, GAS_0 denotes $\mathcal{T} = \{0\}$, i.e., only initial parameters θ_0 are analyzed.

Table 24: *Vision Backdoor Gradient Aggregation*: Adversarial set (\mathcal{D}_{adv}) identification AUPRC mean and standard deviation averaged over ≥ 15 trials for CIFAR10 label pair Auto \rightarrow Dog ($y_{\text{targ}} \rightarrow y_{\text{adv}}$) using Weber et al.’s [70] three attack patterns. Following Weber et al.’s [70] experimental setup, θ_0 was randomly initialized causing GAS₀ as expected to perform poorly. Bold denotes the best mean performance. Mean values are shown graphically in Figure 23a.

$y_{\text{targ}} \rightarrow y_{\text{adv}}$	Attack	GAS ₀	GAS	GAS _T
Auto \rightarrow Dog	1 Pixel	0.043 \pm 0.015	0.982 \pm 0.015	0.909 \pm 0.069
	4 Pixel	0.048 \pm 0.021	0.989 \pm 0.033	0.860 \pm 0.137
	Blend	0.042 \pm 0.021	1 \pm 0	0.999 \pm 0.002

Table 25: *Natural Language Poisoning Gradient Aggregation*: Adversarial set (\mathcal{D}_{adv}) identification AUPRC mean and standard deviation averaged over 10 trials for two positive and two negative SST-2 movie reviews. Bold denotes the best mean performance. Mean values are shown graphically in Figure 23b.

Sentiment	No.	GAS ₀	GAS	GAS _T
Pos.	3	0.789 \pm 0.144	1 \pm 0	0.986 \pm 0.037
	4	0.453 \pm 0.066	1 \pm 0	0.950 \pm 0.083
Neg.	3	0.283 \pm 0.087	0.998 \pm 0.005	0.886 \pm 0.213
	4	0.359 \pm 0.108	1 \pm 0	0.992 \pm 0.025

Table 26: *Vision Poisoning Gradient Aggregation*: Adversarial set (\mathcal{D}_{adv}) identification AUPRC mean and standard deviation averaged over 30 trials for three CIFAR10 class pairs ($y_{\text{targ}} \rightarrow y_{\text{adv}}$) with Zhu et al.’s [77] convex polytope poisoning attack. Bold denotes the best mean performance. Mean values are shown graphically in Figure 23c.

$y_{\text{targ}} \rightarrow y_{\text{adv}}$	GAS ₀	GAS	GAS _T
Bird Dog	0.773 \pm 0.208	0.892 \pm 0.137	0.678 \pm 0.265
Frog Deer	0.912 \pm 0.120	0.962 \pm 0.100	0.837 \pm 0.160
Deer Frog	0.803 \pm 0.188	0.888 \pm 0.091	0.604 \pm 0.234

E.5 Adversarial-Set Identification Execution Time

Recall from Section 4.3 that GAS(-L) is a renormalized version of TracInCP that removes the low-loss penalty. Therefore, GAS(-L)’s execution time is, in essence, that of TracInCP. Table 27 compares the execution time of TracInCP/GAS(-L) to the other influence estimators.²⁶ All results were collected on an HPC system with 3 Intel E5-2690v4 cores, 48GB of 2400MHz DDR4 RAM, and *one* NVIDIA Tesla K80. The reported execution times consider calculating vector \mathbf{v} for training set \mathcal{D}_{tr} w.r.t. a *single* random test example $\hat{\mathbf{z}}_{\text{te}}$. The only exception is the “Amortized” results where training gradient (g_i) computation is amortized across multiple test examples allowing for significant speed-up (see Alg. 1). Amortization relies on simultaneously storing each test example’s gradient \hat{g}_{te} in GPU memory. Therefore, the GPU model constrains amortization’s possible benefits. Table 28 enumerates the number of concurrent test examples considered when calculating amortized results on a K80. More modern GPUs with larger onboard memory see considerable single and amortized speed-ups compared to Table 27.

Recall from Section 6 that natural-language poisoning attacked RoBERTa_{BASE} (125M parameters) as specified by Wallace et al. [68]. Large models can be slow to analyze – even with amortization. That is why natural language target identification uses the two-phase target identification procedure described in Section 5.2. We observed no meaningful performance drop with this streamlined approach (see Figure 7).

Recall from Section 3.2 that Yeh et al.’s [74] representer point estimator only considers the network’s final linear classification layer, which is why it was the fastest. Notably, it also had the worst performance (see Figure 6).

For completeness, Peri et al.’s [50] Deep k -NN empirical clean-label data poisoning defense’s mean execution time was 242s with standard deviation 1.1s.

Target identification execution times can be extrapolated from Table 27’s “Amortized” values.

Table 27: Adversarial-Set Identification Execution Time: Mean and standard deviation algorithm execution time (in seconds) to analyze a single test instance across >50 trials for GAS(-L) and the influence estimator baselines on Section 6.1’s four training-set attacks. See Table 28 for the number of parallel instances analyzed by TracInCP and GAS(-L) for each attack.

Attack	Type	Dataset	TracInCP & GAS(-L)				Others		
			Single		Amortized		TracIn	Inf. Func.	Rep. Pt.
Backdoor	Speech	[43]	2,605 ± 710	489 ± 155	894 ± 279	4,595 ± 177	49 ± 1		
	Vision	CIFAR10	9,252 ± 2,253	1,473 ± 408	2,418 ± 738	6,316 ± 250	128 ± 3		
Poison	NLP	SST-2	27,723 ± 7,933	8,971 ± 3,719	16,667 ± 187	21,409 ± 77	1,697 ± 11		
	Vision	CIFAR10	24,267 ± 1,939	2,088 ± 177	5,910 ± 600	15,634 ± 641	187 ± 2		

Table 28: Single GPU Amortization: Number of test examples analyzed by TracInCP/GAS(-L) when amortizing on an Nvidia Tesla K80 computation of training gradients (g_i) in Table 27’s “Amortized” execution time result.

Attack	Type	
Backdoor	Speech	20
	Vision	16
Poison	NLP	5
	Vision	135

²⁶Table 27 does not separately report GAS and GAS-L’s execution times as they were consistently similar to TracInCP.